

**Nonlinear Model Predictive Control (NMPC) for
Twin Rotor MIMO System (TRMS)**

by

Cheah Zong Yuan

16242

Dissertation submitted in partial fulfilment of

the requirements for the

Bachelor of Engineering (Hons)

(Electrical and Electronics)

JANUARY 2016

Universiti Teknologi PETRONAS

Bandar Seri Iskandar

31750 Tronoh

Perak Darul Ridzuan

CERTIFICATION OF APPROVAL

**Nonlinear Model Predictive Control (NMPC) for
Twin Rotor MIMO System (TRMS)**

by

Cheah Zong Yuan

16242

A project dissertation submitted to the
Electrical and Electronics Engineering Programme
Universiti Teknologi PETRONAS
in partial fulfilment of the requirement for the
BACHELOR OF ENGINEERING (Hons)
(ELECTRICAL AND ELECTRONICS)

Approved by,

(Ir Dr Idris bin Ismail)

UNIVERSITI TEKNOLOGI PETRONAS
TRONOH, PERAK

January 2016

CERTIFICATION OF ORIGINALITY

This is to certify that I am responsible for the work submitted in this project, that the original work is my own except as specified in the references and acknowledgements, and that the original work contained herein have not been undertaken or done by unspecified sources or persons.

CHEAH ZONG YUAN

ABSTRACT

Twin Rotor MIMO System (TRMS) is a dynamic model with high non-linearity that resembles a helicopter with reduced degree-of-freedom (DOF). Besides, cross-coupling between main rotor and tail rotor contributes to the difficulty in controlling the system. Majority of the previous researches have not focused on continuous actual dynamic disturbance test. The objectives of this project are to model TRMS and control the system against major disturbance (wind effect) and set-point changes. The first phase of the project started with mathematical modelling of direct current (DC) motors, where the relationship between input voltage and angular velocity was captured. The next phase would be the modelling of the whole system and design of controller. During the second phase, the modelling would involve aerodynamics and other Physics laws. Once the complete model was formed, Proportional, Integral and Derivative (PID) and Linear Quadratic Regulator (LQR) controllers were designed to optimize the dynamic system. The system has been tested using wind variation as actual dynamic disturbance to validate the disturbance rejection performance. It was found that the best performance from combination of PID and LQR controllers gave 89% improvement in term of pitch overshoot and 33% improvement in term of yaw overshoot during disturbance rejection compared to PID-only controller.

ACKNOWLEDGEMENTS

First and foremost, the author would like to express deepest gratitude to Ir Dr Idris bin Ismail, who has been giving the effort in coordinating throughout the project. Knowledge sharing and guidance from him had contributed a lot to the completion of this project. Besides, the author owed many thanks to Mr Nguyen Tuan Hung and Mr Tho Dang Huu for giving technical assistances on TRMS.

In addition, a great thank you was acknowledged to Universiti Teknologi PETRONAS for providing the facilities needed for the completion of project. The availability of TRMS unit in the lab and updated software made the completion of project possible. Last but not least, the author would like to take this opportunity to thank his family and friends for their continuous support and encouragement.

LIST OF ABBREVIATIONS

NMPC: Nonlinear Model Predictive Control
MIMO: multi-input multi-output
TRMS: Twin Rotor MIMO System
DC: direct current
DOF: degree-of-freedom
PID: Proportional, Integral and Derivative
NMHE: Nonlinear Moving Horizon Estimation
MPC: Model Predictive Control
LQR: Linear Quadratic Regulator

LIST OF NOMENCLATURES

x state/ closed-loop states
 \dot{x} first derivative of x
 \bar{x} predicted state
 x_s targeted state
 u input/ closed-loop input
 \bar{u} open loop input
 u_s targeted input
 t time
 \mathbb{R} real number
 J cost function
 F stage cost function
 T_p prediction horizon
 T_c control horizon

LIST OF TABLES

Table A - 1: Data collected from main rotor experiment38
Table A - 2: Data collected from main rotor experiment40

LIST OF FIGURES

Figure 1: Schematic of an articulated rotor hub and root	2
Figure 2: Schematic of the rotor swash plate.....	2
Figure 3: TRMS unit used in this project [9].....	3
Figure 4: TRMS simplified system schematic.....	3
Figure 5: General NMPC calculation procedures	7
Figure 6: Principle of MPC	7
Figure 7: Block diagram of Linear Quadratic Regulator.....	9
Figure 8: Block diagram of complete system	11
Figure 9: Experiment setup for measurement using digital tachometer.....	13
Figure 10: Experiment setup for measurement using dc tachometer	13
Figure 11: Overall project flow	14
Figure 12: Wind source applied from x_1 to x_2	16
Figure 13: Table fan at top of pitch rotor	16
Figure 14: Table fan at side of yaw rotor	16
Figure 15: Table fan at top of yaw rotor.....	16
Figure 16: Measured and simulated model output for main pitch model.....	19
Figure 17: Measured and simulated model output for cross pitch model.....	20
Figure 18: Measured and simulated model output for main yaw model.....	21
Figure 19: Measured and simulated model output for cross yaw model.....	22
Figure 20: Complete TRMS model.....	23
Figure 21: Setpoint tracking in simulation (PID).....	26
Figure 22: Setpoint tracking in simulation (PID+LQR).....	26
Figure 23: Setpoint tracking in real-time (PID).....	27
Figure 24: Setpoint tracking in real-time (PID+LQR)	28
Figure 25: Disturbance rejection part 1 (PID)	28
Figure 26: Disturbance rejection part 1 (PID+LQR)	29
Figure 27: Disturbance rejection part 2 (PID)	29
Figure 28: Disturbance rejection part 2 (PID+LQR)	30
Figure 29: Disturbance rejection part 3 (PID)	30
Figure 30: Disturbance rejection part 3 (PID+LQR)	31
Figure 31: Disturbance rejection part 4 (PID)	31
Figure 32: Disturbance rejection part 4 (PID+LQR)	32
Figure A - 1: Project Timeline and Key Milestones	37
Figure A - 2: Comparison of measured angular velocity between digital tachometer and DC tachometer	39
Figure A - 3: Comparison of measured angular velocity between digital tachometer and DC tachometer	39
Figure A - 4: Transfer function models of main rotor.....	41
Figure A - 5: State-space models of main rotor (ss1 & ss2).....	42
Figure A - 6: State-space models of main rotor (ss1, ss2, ss3 & ss4)	42
Figure A - 7: Transfer function models of tail rotor	44
Figure A - 8: State-space models of tail rotor.....	45

TABLE OF CONTENTS

ABSTRACT	i
ACKNOWLEDGEMENTS	ii
LIST OF ABBREVIATIONS	iii
LIST OF NOMENCLATURES	iii
LIST OF TABLES	iii
LIST OF FIGURES	iv
CHAPTER 1: INTRODUCTION	1
1.1. Background of Study	1
1.2. Problem Statement	4
1.3. Objectives	4
CHAPTER 2: LITERATURE REVIEW AND THEORY	5
2.1. Previous Works	5
2.2. Nonlinear Model Predictive Control (NMPC)	6
2.2.1. General overview	6
2.2.2. Algorithm	7
2.3. Linear Quadratic Regulator (LQR)	9
CHAPTER 3: RESEARCH METHODOLOGY	10
3.1. Methodology	10
3.2. Experiment – Relationship between input voltage and angular velocity	11
3.3. Experiment – Disturbance rejection	15
3.4. Project Timeline and Key Milestones	15
CHAPTER 4: RESULTS AND DISCUSSION	17
4.1. System representation of TRMS	17
4.1.1. Main pitch model	17
4.1.2. Cross pitch model	18
4.1.3. Main yaw model	18
4.1.4. Cross yaw model	18
4.1.5. Complete TRMS model	23
4.2. Controller design	23
4.2.1. PID tuning	23
4.2.2. LQR tuning	24
4.2.3. Simulation	25

4.3.	Field test	27
4.3.1.	Setpoint tracking	27
4.3.2.	Disturbance rejection part 1: wind source from x1 to x2	28
4.3.3.	Disturbance rejection part 2: wind source from z1 to z2	29
4.3.4.	Disturbance rejection part 3: wind source from x3 to x4	30
4.3.5.	Disturbance rejection part 4: wind source from z3 to z4	31
CHAPTER 5: CONCLUSION		33
5.1.	Conclusion	33
5.2.	Recommendations	34
REFERENCES		35
APPENDICES		37
A.1.	Project timeline and key milestones	37
A.2.	Data collected from main rotor	38
A.3.	Data collected from tail rotor	39
A.4.	Model identification of rotors	40
A.4.1.	Transfer function model of main rotor	41
A.4.2.	State-space model for main rotor	42
A.4.3.	Transfer function model for tail rotor	43
A.4.4.	State-space model for tail rotor	44

CHAPTER 1

INTRODUCTION

1. INTRODUCTION

1.1. Background of Study

A helicopter is a type of aircraft that uses propulsive forces created from rotating blades to travel [1]. The rotation of main rotor blades around vertical axis on high angular velocity forms a virtually horizontal disk which provides thrust to lift up the helicopter. In addition, there is a significant motion on the hinged blades as shown in **Figure 1**, which can alter the stress on the blades or momentum on the root by the means of angle of attack on the blades. Both collective pitch control and cyclic pitch control can be achieved through swash plate mechanism as shown in **Figure 2** [2]. Collective pitch control works by changing the pitch of all the rotor blades at the same time to cause a climb or descent while cyclic pitch control allows the helicopter to move in certain direction by changing the pitch angle of rotor blades at corresponding point of the rotation plane. The stability of helicopter in forward flight is achieved by the horizontal thrust produced by rotating tail rotor [3].

Application of the concept of Nonlinear Model Predictive Control (NMPC) on multi-input multi-output (MIMO) system can be studied through TRMS which is a dynamic model that resembles a helicopter [4]. However, the operation method in TRMS is slightly different from the real helicopter. There is no swash plate mechanism in TRMS and the only way to control the elevation is by changing the angular velocity of main rotor. The functionality of tail rotor for both helicopter and TRMS remains the same. TRMS was developed by Feedback Instruments for experimentation on modelling and control [5] and the mechanical structure was shown in **Figure 3**. Two

rotors are mounted perpendicular to each other. The pitch rotor, is responsible in producing vertical thrust while the yaw rotor produces horizontal thrust to the model. The rotors are connected to a beam and the beam is pivoted to a tower. With the beam pivoted to a tower, TRMS is reduced to 2 DOF. In order to bring equilibrium point to the model, there is a counterweight attached to the middle point of the beam.

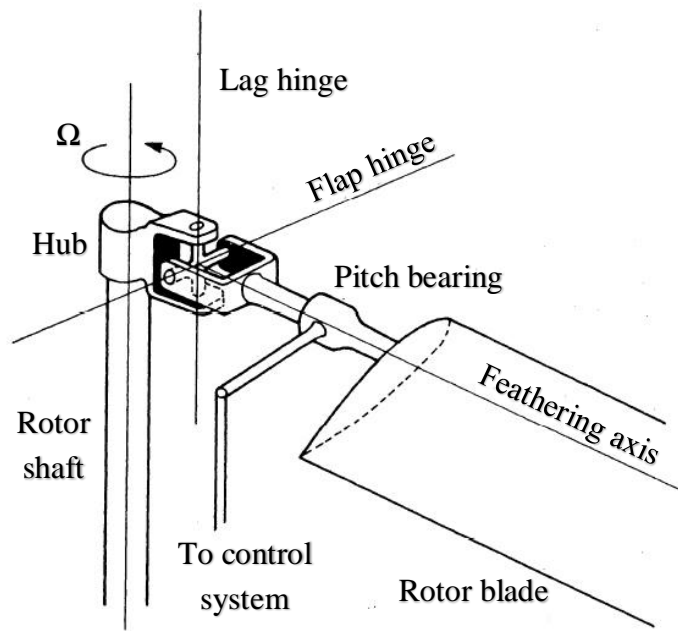


Figure 1: Schematic of an articulated rotor hub and root

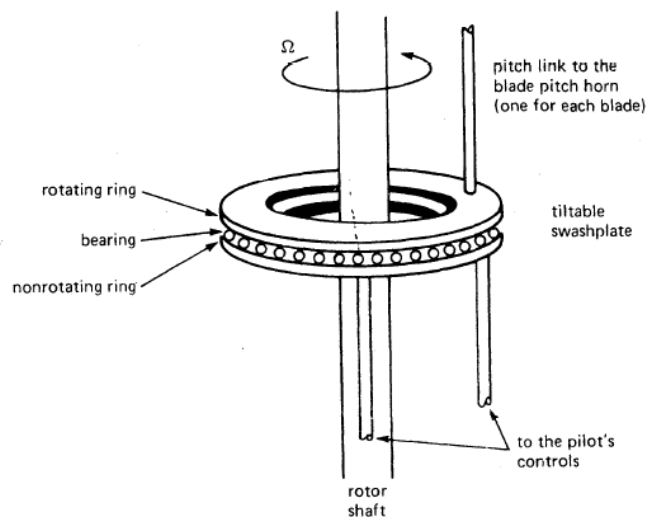


Figure 2: Schematic of the rotor swash plate

Although it is a simplified model of a helicopter, non-linearity and cross-coupling between subsystems in the model as shown in **Figure 4** are still giving significant challenges in extracting the model. The two main subsystems here are the main rotor and tail rotor; the whole system reacts as the impact from these two rotors. In previous study done by Aldebrez *et al.*, the modelling of the system started off with system identification which was said to be the most important stage for getting the model to solve problems [6]. Laws of physics such as electromagnetic and aerodynamics can be found on TRMS, hence the structure of the model can be captured through first principle modelling [7]. Missing parameters are to be found from experimentation and specification table provided by Feedback Instruments. Christensen *et al.* implemented linearization using Taylor series expansion to convert nonlinear parameters to linear form [8]. Controllers can be designed once the transfer functions of each component are found and linked to form the final model.

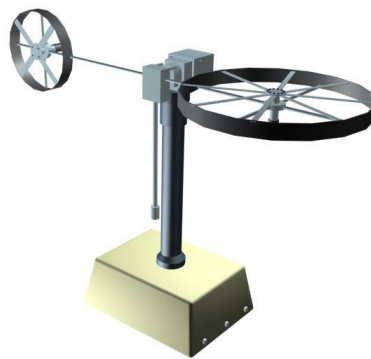


Figure 3: TRMS unit used in this project [9]

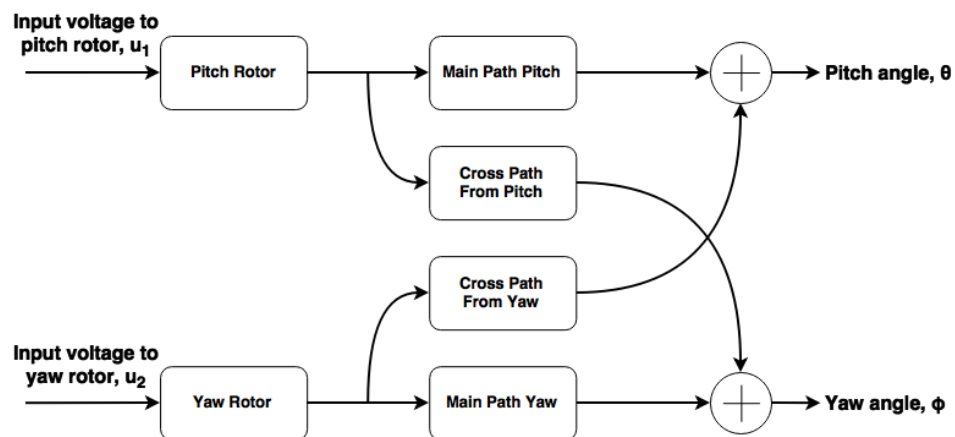


Figure 4: TRMS simplified system schematic

1.2. Problem Statement

High degree of non-linearity and cross-coupling between variables are the factors that make the TRMS hard to be modelled and controlled. The cross-coupling mainly comes from the main rotor and tail rotor. In order to get the TRMS to operate under highly reliable performance, an appropriate control mechanism is required to be implemented to the system. More importantly, the controller must be capable of tackling the high non-linearity and cross-coupling within the system.

Other than that, robustness is also a crucial aspect in TRMS. In this project, capability to reject disturbances such as wind and external forces is being concerned. The stability of TRMS is highly related to disturbance rejection as it defines the performance of TRMS under adverse condition. It was found that previous controller designs as stated in literature review are either involved complex computation or non-robust.

1.3. Objectives

The objectives of carrying out this project are:

- 1) To construct the mathematical model of TRMS.
- 2) To control TRMS:
 - against major disturbance by testing against actual wind variation (disturbance rejection).
 - against set-point changes (set-point tracking).

The scope of this project is limited to the TRMS structure used in the university. Manipulated variables in this system are the input voltage to pitch rotor and input voltage to yaw rotor while the controlled variables are the pitch angle and yaw angle. The system should be able to hover in the air and stand against disturbances like wind or external forces applied to the structure. When there is an unexpected force applied to it and changes its flying direction, it should be able to go back to the desired position.

CHAPTER 2

LITERATURE REVIEW AND THEORY

2. LITERATURE REVIEW AND THEORY

2.1. Previous Works

Recent study [10] had demonstrated the design of two fuzzy logic controllers to control the TRMS. The controllers were designed based on decent gradient algorithm. The advantage of using fuzzy logic is that it does not require the implementation of differential equation, which makes the design of controller much easier. In term of set-point tracking, the controller for main part performed better than that of tail part. Disturbance was introduced in real time to the system and it was found that the controller in main part showed better disturbance rejection. In neural network approach done in, black-box modelling did not show completely the relationship between variables involved in the process [11]. However, neural network gained a satisfying performance and outperformed the PID controller.

There was also an approach done using classical control, for instance, Proportional, Integral and Derivative (PID) control on TRMS was implemented in [12]. A simple PID controller together with a cross-coupled PID controller were designed and the performances of TRMS after implementation of controllers were evaluated. From the experimental results, it can be seen that set-point tracking is not performing well. The overall performance gave a high degree of error and it can be concluded that PID is not a suitable control method for TRMS with high non-linearity and cross-coupling.

Disturbance rejection tests were done in [13] and [14] by using software implementation of disturbance. However, the results cannot represent the performance in real-time as the response in real system is affected by multiple unpredictable environmental variables. Actual implementation of disturbance at the yaw rotor was carried out in [15], but there is no experimental result for pitch rotor part.

2.2. Nonlinear Model Predictive Control (NMPC)

2.2.1. General overview

In general, a control system is designed to stabilize a feedback system while satisfying the constraints [16]. Most of the applications in real world are nonlinear, which means the output does not show a directly proportional behaviour towards the input. NMPC or some referred it as Nonlinear Moving Horizon Estimation (NMHE) can be an effective solution to control the nonlinear system [17]. Badgwell *et al.* has characterized the general NMPC calculation procedures as **Figure 5**. The working mechanism behind this control method is basically the estimation of behaviour of a system in the future and implementation of controller to optimize the system [18]. Besides, it has several advantages over other control methods in term of capability to work directly on important variables of a system, control the system in the sense of predicting the future response and cope within constraints.

As superposition principle is no longer valid on nonlinear model [19], the derivation of dynamic model could not be done solely by ordinary system identification, data from measurements or experiments are required to fill the unknown parametric values. Validation step should be carried out on the model before it is being utilized for controller design. One systematic way of performing the validation is by running the model and justifies the feasibility of the model by analyzing the deviation found between measured output and predicted response. Upon getting the accurate dynamic model, the controller calculates for predicted future behaviour and identifies an optimum input to optimize the system. NMPC controller was commonly configured along with a state observer to ensure the stability of the system [20]. NMPC is

formulated to provide solution to optimal control problems repetitively and the optimization process occurs at each sampling instant [21]. All the advantages mentioned above showed that NMPC is a suitable mechanism to control TRMS in this project.

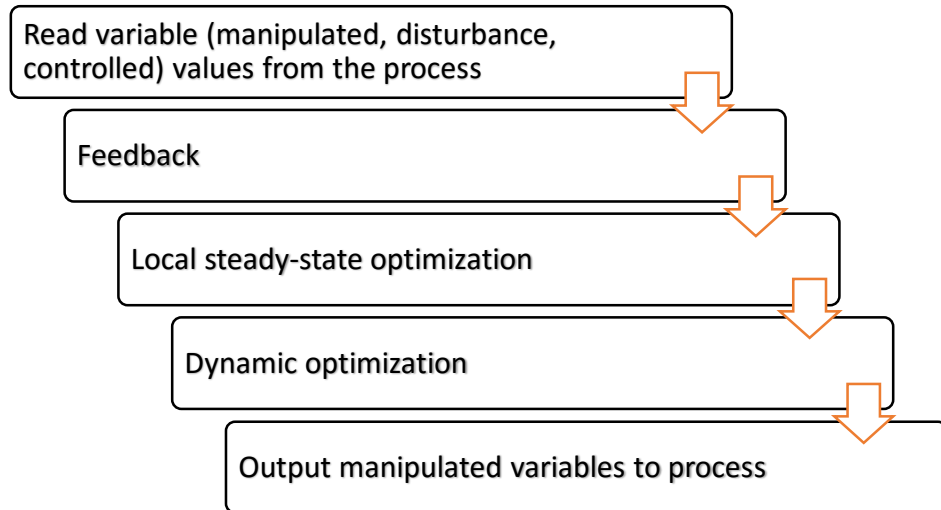


Figure 5: General NMPC calculation procedures

2.2.2. Algorithm

NMPC as an extension from Model Predictive Control (MPC) runs on the same algorithm as the parent except that the application is now on nonlinear processes [22].

Figure 6 shows the principle of MPC in graphical form.

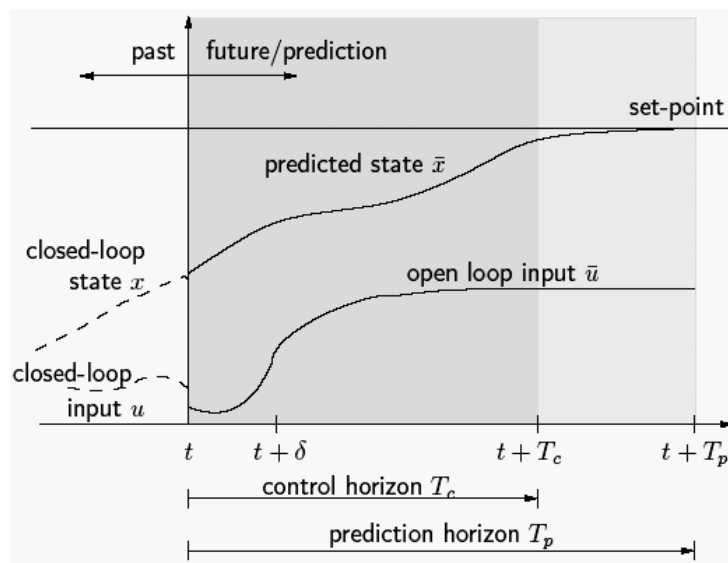


Figure 6: Principle of MPC [23]

A nonlinear system can be commonly presented in an equation where first derivative of $x(t)$ [$\dot{x}(t)$] is a function of input, $u(t)$ and state, $x(t)$, with initial condition, $x(0)$, as shown below:

$$\dot{x}(t) = f(x(t), u(t)), x(0) = x_0 \quad (1)$$

subject to input and state constraints:

$$u(t) \in U, \forall t \geq 0 \quad (2)$$

$$x(t) \in X, \forall t \geq 0 \quad (3)$$

where U and X are normally bounded within different sets of real number, \mathbb{R} :

$$U := u \in \mathbb{R}^m | u_{\min} \leq u < u_{\max} \quad (4)$$

$$X := x \in \mathbb{R}^n | x_{\min} \leq x < x_{\max} \quad (5)$$

NMPC can be introduced into a finite horizon optimization problem in term of minimizing cost function. The cost function, J , can be expressed as:

$$J(x(t), \bar{u}(\cdot)) := \int_t^{t+T_p} F(\bar{x}(\tau), \bar{u}(\tau)) d\tau \quad (6)$$

where

\bar{u} is the open loop input

\bar{x} is the predicted state

subject to:

$$\dot{\bar{x}}(\tau) = f(\bar{x}(\tau), \bar{u}(\tau)), \bar{x}(t) = x(t) \quad (7)$$

$$\bar{u}(\tau) \in U, \forall \tau \in [t, t + T_c] \quad (8)$$

$$\bar{u}(\tau) = \bar{u}(t + T_c), \forall \tau \in [t + T_c, t + T_p] \quad (9)$$

$$\bar{x}(\tau) \in X, \forall \tau \in [t, t + T_p] \quad (10)$$

T_c denotes control horizon while T_p denotes prediction horizon with the condition of $T_c \leq T_p$. The performance in term of cost can be reflected through stage cost function, F , which is commonly expressed in quadratic form:

$$F(x, u) = (x - x_s)^T Q (x - x_s) + (u - u_s)^T R (u - u_s) \quad (11)$$

with x_s and u_s denoting targeted values in state and input respectively. The weightage of deviation is presented in matrices Q and R with the condition $Q>0, R>0$.

2.3. Linear Quadratic Regulator (LQR)

LQR runs on the principle of optimal control at minimized quadratic cost function [24]. It was chosen as the controller to implement NMPC on TRMS because the operation of LQR matches the working principle of NMPC, specifically prediction of states and minimization of cost function. LQR uses the control strategy that offers optimal and stable response in the output of the system [25]. The computation of state feedback gain matrix K is depending on the state weighting matrix Q and the control weighting matrix R [26]. The state feedback gain matrix K can be determined using the following equation:

$$K = R^{-1}B^T P \quad (12)$$

provided that matrix P was obtained by solving Riccati equation [27]:

$$A^T P + PA - PBR^{-1}B^T P + Q = 0 \quad (13)$$

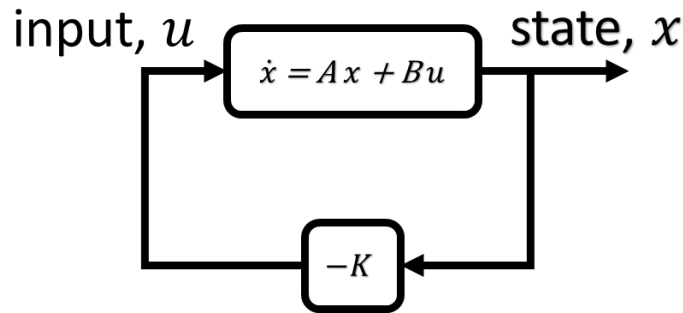


Figure 7: Block diagram of Linear Quadratic Regulator

CHAPTER 3

RESEARCH METHODOLOGY

3. RESEARCH METHODOLOGY

3.1. Methodology

TRMS is being used in this project to study the behaviour of a nonlinear system with reduced degree of freedom. The angular velocity of the blades is depending on the voltage applied to the rotor, hence the modelling should start from the relationship between supply voltage and the rotor. Basic mathematical equations related to electromagnetic theory can be used as reference here. In the next stage, a series of experiments were carried out to obtain the relationship between the input voltage and resultant angular displacement for both pitch rotor and yaw rotor. The 4th run of this experiment was meant to be aggressive and it was carried out with random input signal having higher variance compared to the other runs. From the relationship between respective input voltage and angular displacement, transfer function for main pitch path, cross pitch path, main yaw path and cross yaw path were estimated through simulation. Each of the models obtained from system identification were then validated against respective actual output from the 4 runs of experiment. In the end of modelling stage, a full model of TRMS was formed and ready to be used for controller design.

In controller design stage, PID controller was designed using Ziegler-Nichols closed-loop tuning method. Parameters of the gains (K_p , K_i , K_d) were determined and fine-tuned through this method. Besides, LQR was being designed to work together with PID controller and the overall block diagram of the complete system can be referred from Figure 8. LQR is an optimal controller which provides the smallest possible error to its input. Even for a multivariable system, LQR is still straightforward to use; the design procedure is essentially the same as for single-input-

single-output systems. However, LQR is only applicable if the system is state controllable. The steps in designing LQR can be outlined as below:

- 1) Choose for the values of Q and R.
- 2) Find the value P by solving Equation (13).
- 3) Compute for the value K by using Equation (12).
- 4) Implement $u = -Kx$ in the feedback system.
- 5) Simulate the initial response of $\dot{x} = (A - BK)x$ for different initial conditions.
- 6) If the transient response specifications and/or the magnitude constraints are not met, go back to step 1 and fine-tune Q and/or R.

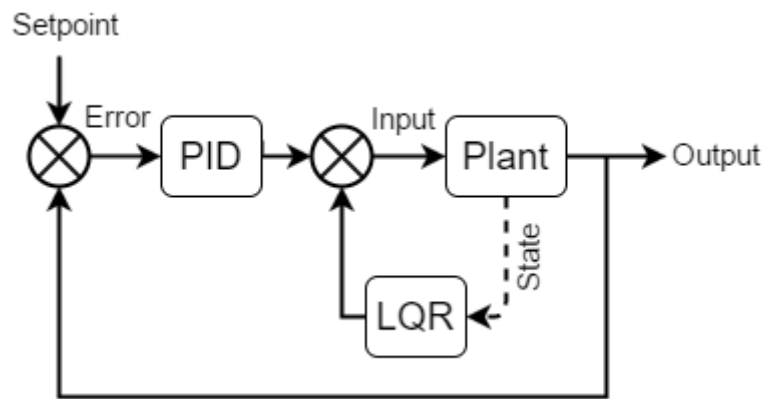


Figure 8: Block diagram of complete system

The final stage of this project was the field test. PID and LQR controllers were implemented on TRMS to verify that the performance of the system meets the requirements. Depending on the result obtained, the controllers were further fine-tuned for better improvement. The overall project flow can be studied from **Figure 11**.

3.2. Experiment – Relationship between input voltage and angular velocity

Experiments were done on main rotor and tail rotor to get the data regarding relationship between input voltage and angular velocity. Data of angular velocity were collected through both digital tachometer and DC tachometer. After the experiment was completed, the data from digital tachometer were used to verify the reliability of data from DC tachometer. The procedures of experiment for main rotor were outlined in Part A while the procedures of experiment for tail rotor were outline in Part B.

Part A: Main Rotor

- 1) Through Advantech Device Manager, the computer produces analog output signal ranging from 0V to 5V (in signed value, it is from -2.5V to 2.5V).
- 2) The signal is then amplified to a value ranging from -20V to 20V, which is the voltage for main rotor to run.
- 3) The rotational speed of main rotor was measured using a digital tachometer and dc tachometer.
- 4) The results were tabulated in **Table A - 1** and analysed.

Part B: Tail Rotor

- 1) Through Advantech Device Manager, the computer produces analog output signal ranging from 0V to 5V (in signed value, it is from -2.5V to 2.5V).
- 2) The signal is then amplified to a value ranging from -15V to 15V, which is the voltage for tail rotor to run.
- 3) The rotational speed of tail rotor was measured using a digital tachometer and dc tachometer.
- 4) The results were tabulated in **Table A - 2** and analysed.

Figure 9 shows the experiment setup for measurement of rotational speed using a digital tachometer. When taking readings of rotational speed, the digital tachometer should be pointed perpendicular to the rotating disc. The DC tachometer is attached next to the DC motor and can be found on both main rotor and tail rotor. The output of DC tachometer can be obtained from connector labelled PL2 at the interface circuit as shown in **Figure 10**.

Notes:

- 1) Output measured between pin 1 & 2 is the DC tachometer output for tail rotor.
- 2) Output measured between pin 3 & 4 is the DC tachometer output for main rotor.
- 3) Specification of DC tachometer: 0.52V per 1000 RPM.

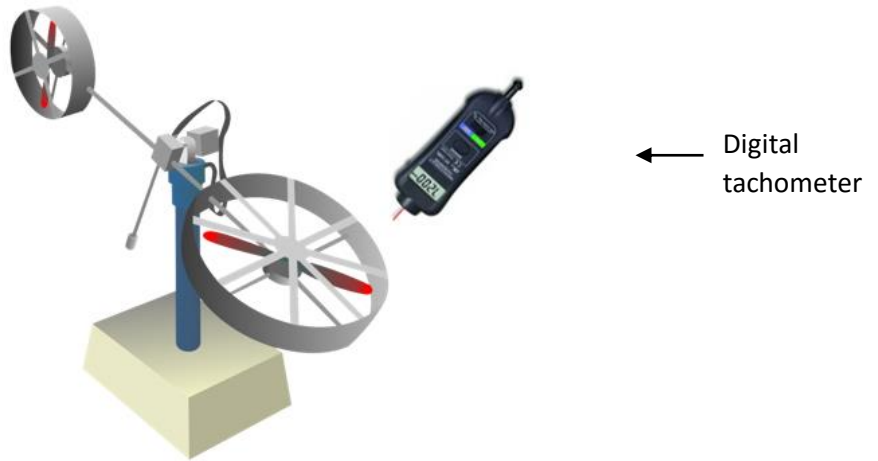


Figure 9: Experiment setup for measurement using digital tachometer

Note: Data obtained from digital tachometer were divided by 2 as there were 2 blades rotating together.

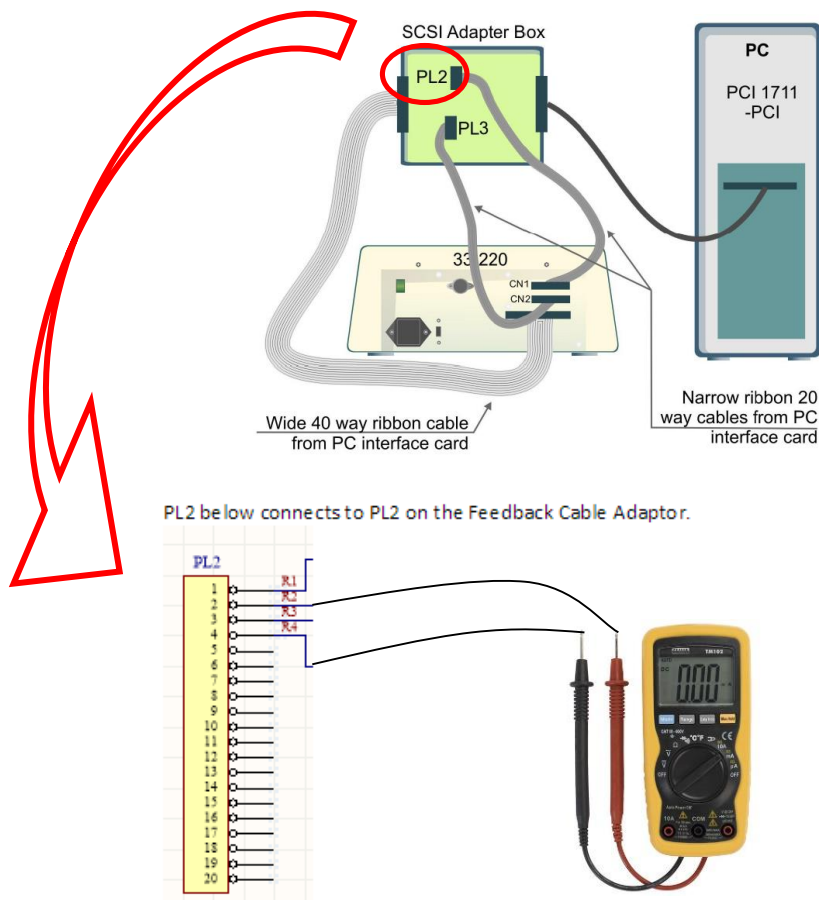


Figure 10: Experiment setup for measurement using dc tachometer

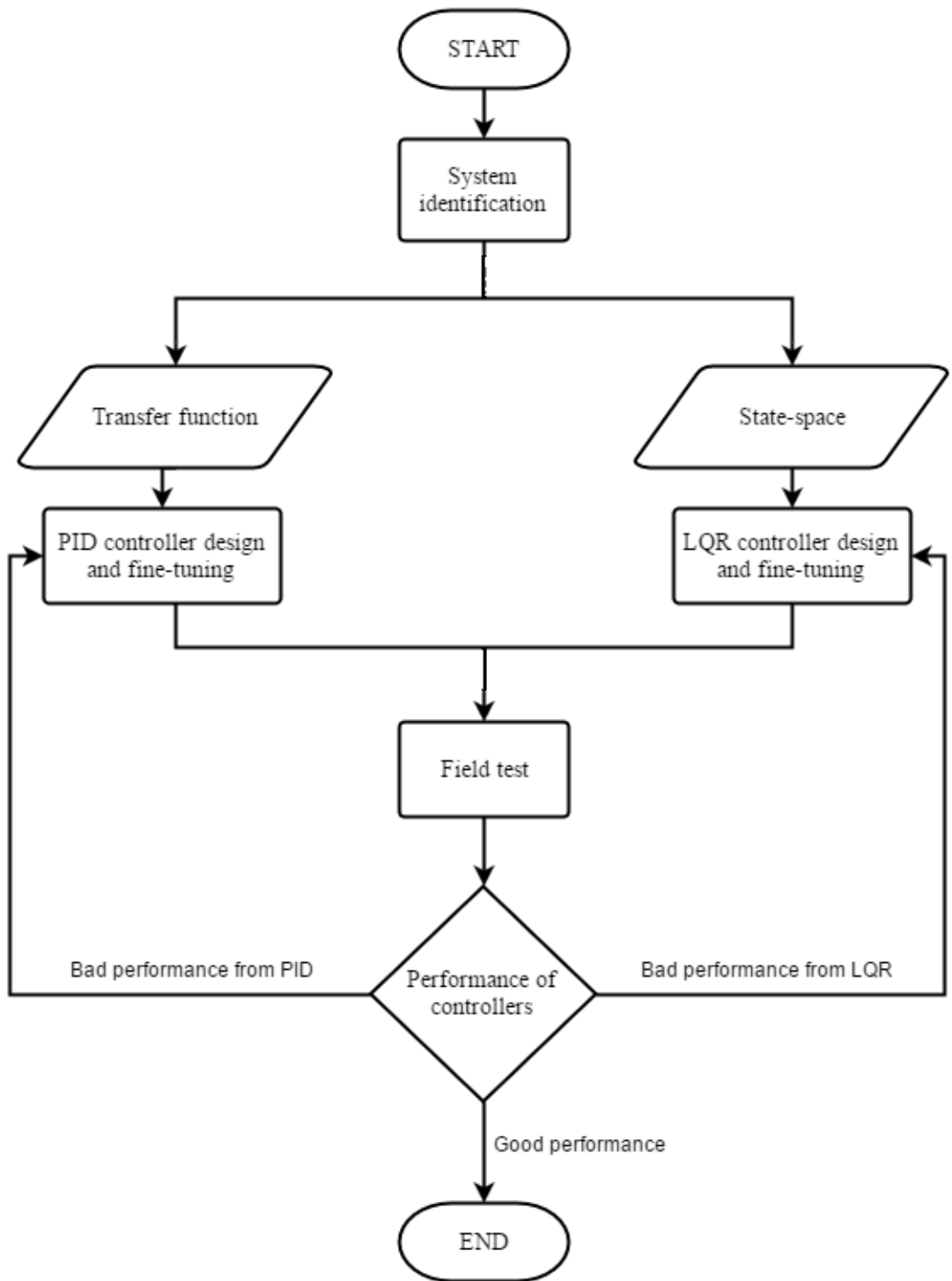


Figure 11: Overall project flow

3.3. Experiment – Disturbance rejection

Wind source from a table fan was used to simulate the disturbance to the TRMS in real-time. The disturbance rejection experiment started after both the pitch angle and yaw angle reached the desired setpoints, where in this case the setpoint of pitch angle is at 0.45 rad while the setpoint of yaw angle is at 0.4 rad. There is a total of 4 parts throughout the experiment, each with different direction of the wind, which are:

- 1) from x_1 to x_2 (**Figure 12**)
- 2) from z_1 to z_2 (**Figure 13**)
- 3) from x_3 to x_4 (**Figure 14**)
- 4) from z_3 to z_4 (**Figure 15**)

In part 1, the wind from a table fan was applied towards the side of pitch rotor at 30th second and elapsed for 20 seconds before being removed. After the first part was done, the experiment was continued with the next part until all 4 parts were completed. The responses from the real-time experiment were collected and plotted in graphs.

3.4. Project Timeline and Key Milestones

Final year project was secured during the first week with the title of “Nonlinear Model Predictive Control (NMPC) for Twin Rotor MIMO System (TRMS)”. The first phase of the project was started with background study on the topic through in-depth literature review. The study was emphasized around the application of NMPC on TRMS and it was done for about 6 weeks long. LQR as the proposed method was studied along to understand the principle and algorithm. An extended proposal containing details on the project was prepared and submitted on Week 6. After that, the modelling of DC motors was started. An experiment setup was proposed to obtain data for system representation purpose and it was done for both main rotor and tail rotor. Upon getting the required data, the data was used to create models for both main rotor and tail rotor in the form of transfer function and state-space. The responses given by the models were then further verified with the data obtained. The first phase of the project ended with final models for both main rotor and tail rotor. An interim report

containing the works done and results during first phase of project was submitted before the semester ended.

In the second phase of project, the modelling work continues for whole TRMS structure. Physics laws and cross-coupling are taking place in the model, making the modelling process harder than phase 1. The final model was formed by the end of Week 7. Once the model of TRMS is formed, PID controller and LQR controller were designed to control the system for better performance. The controllers were then implemented to the system and tested for both setpoint tracking and disturbance rejection. Towards the end of Week 11 during FYP2, the combination of PID controller and LQR controller was found to be giving reliable performance to the TRMS. Eventually, the project was ended with a complete TRMS model together with functional controllers. By the end of FYP2, all the documentations were organized and a dissertation was submitted to examiners.

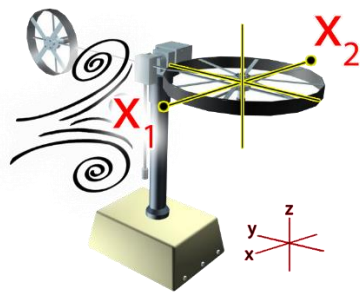


Figure 12: Wind source applied from x_1 to x_2

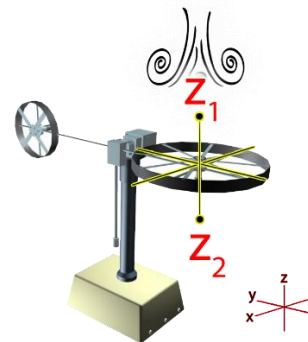


Figure 13: Table fan at top of pitch rotor

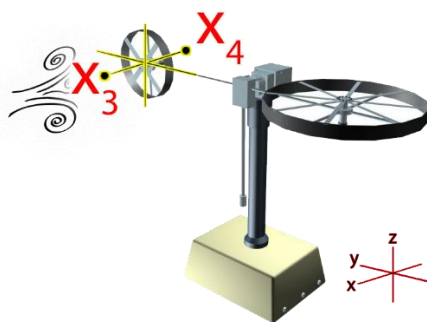


Figure 14: Table fan at side of yaw rotor

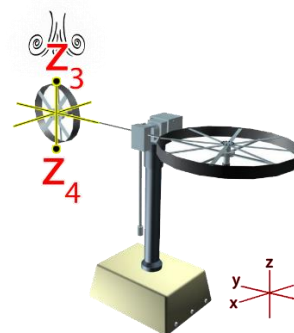


Figure 15: Table fan at top of yaw rotor

CHAPTER 4

RESULTS AND DISCUSSION

4. RESULTS AND DISCUSSION

4.1. System representation of TRMS

Experiments were carried out by applying multisinusoidal signal to excite the TRMS model. The responses in term of pitch angle and yaw angle were collected in the form of vectors and used for estimation of model.

4.1.1. Main pitch model

By referring to the relationships between input voltage to the main rotor and pitch angle shown in **Figure 16**, the best transfer function that can represent the system well was found. By calculating for average best fit scores, the transfer function that can represent the main pitch section is tf7, which is in the form of:

$$\frac{0.1719s^6+1.515s^5+2.417s^4+5.198s^3+4.523s^2+0.5371s+0.01648}{s^7+1.134s^6+7.446s^5+6.78s^4+14.02s^3+9.203s^2+1.231s+0.0408} \quad (14)$$

4.1.2. Cross pitch model

The transfer function that can represent cross pitch model was found from the result shown in Figure 17 by calculating the average best fit scores. It was found that the transfer function that best represent the cross pitch section is tf8, which is in the form of:

$$\frac{-0.09933s^7+0.6608s^6+0.003581s^5+0.2009s^4+0.006373s^3+0.0111s^2+0.0004691s+9.821e-07}{s^8+0.8412s^7+0.8136s^6+0.2882s^5+0.1634s^4+0.02336s^3+0.007168s^2+0.0005429s+1.396e-07} \quad (15)$$

4.1.3. Main yaw model

Based on the result shown in Figure 18, it was found that tf8 is having the highest average best fit scores. Thus, tf8 is the transfer function that can represent main yaw section and it is in the form of:

$$\frac{0.2956s^7-0.04341s^6+1.889s^5+0.1563s^4+0.6762s^3+0.03422s^2+0.01223s+8.886e-05}{s^8+4.745s^7+2.185s^6+3.1s^5+0.6928s^4+0.5212s^3+0.03725s^2+0.00793s+9.146e-05} \quad (16)$$

4.1.4. Cross yaw model

By referring to the measured and simulated model outputs shown in Figure 19, the best transfer function that can represent the system well was found by calculating for average best fit scores. It was found that cross yaw section can be represented by tf7, which scored the highest in average best fit scores. The transfer function model of cross yaw section can be written as:

$$\frac{0.1648s^6+0.03416s^5+0.7467s^4+0.1508s^3+0.2388s^2-0.02808s-0.00046}{s^7+0.6482s^6+8.889s^5+4.815s^4+19.94s^3+8.704s^2+0.9414s+0.0126} \quad (17)$$

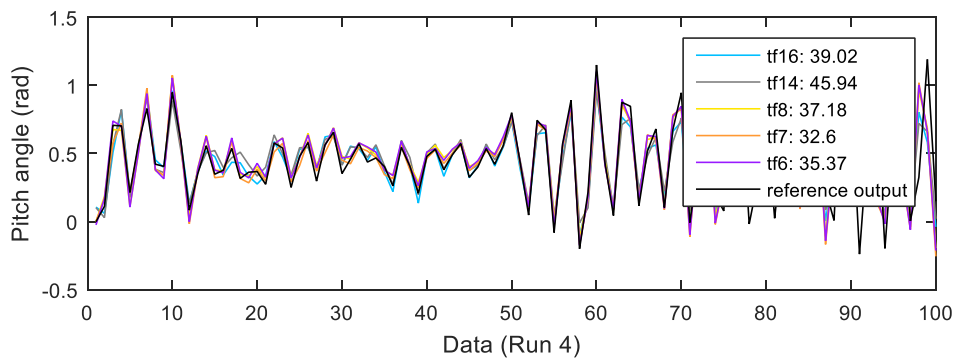
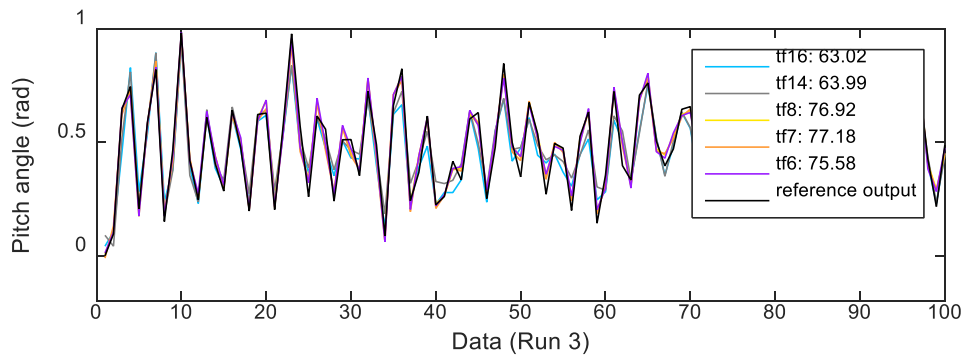
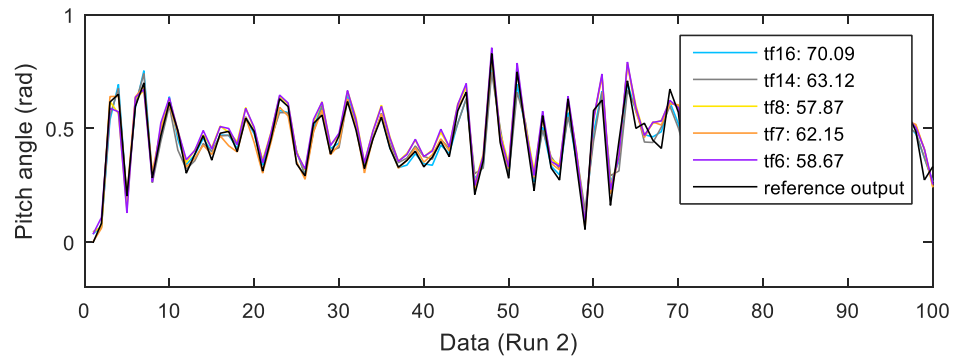
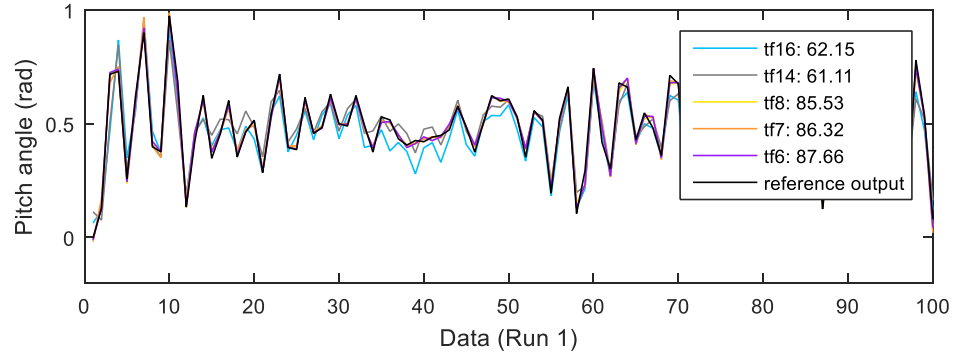


Figure 16: Measured and simulated model output for main pitch model

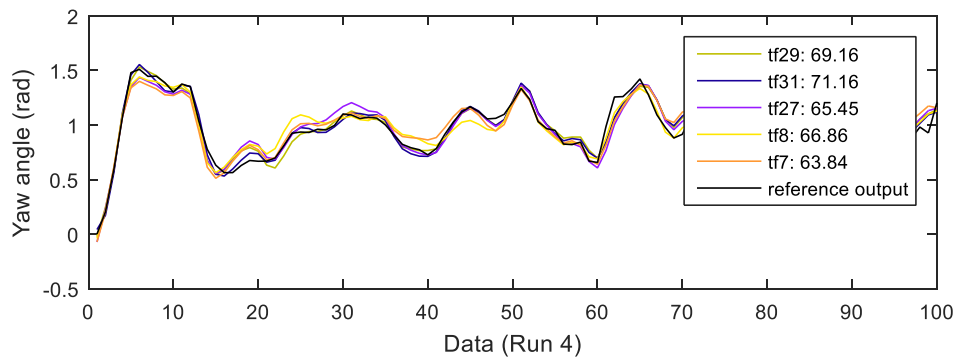
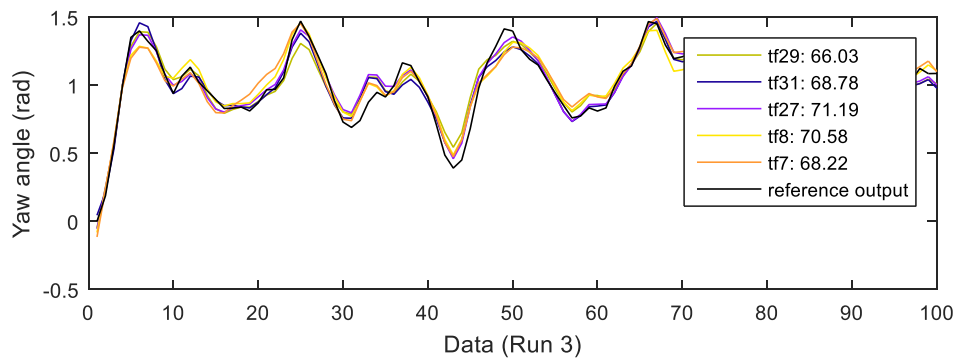
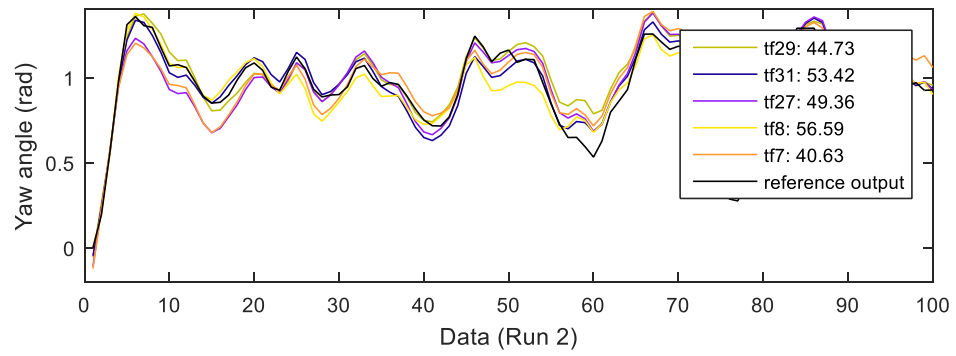
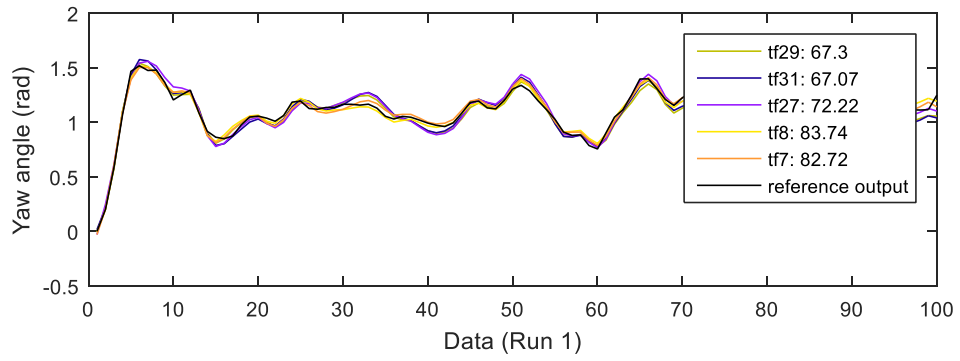


Figure 17: Measured and simulated model output for cross pitch model

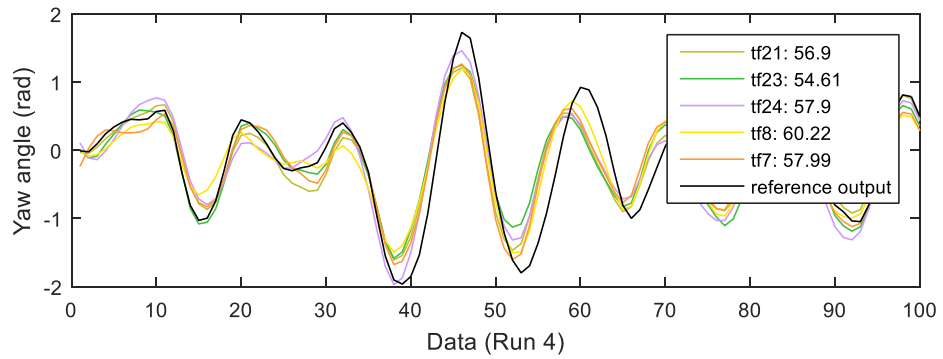
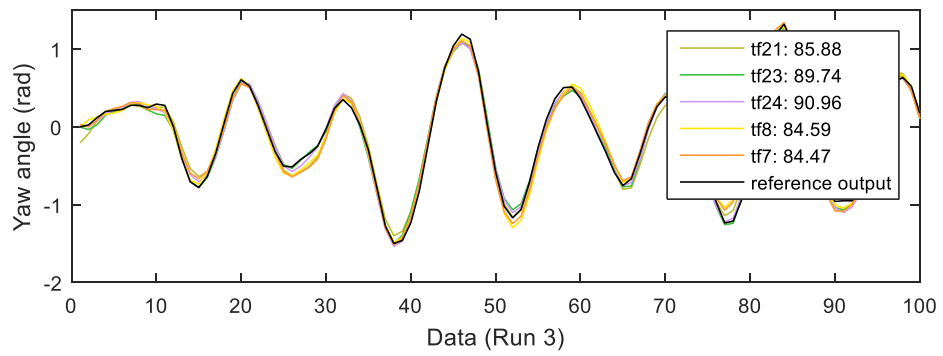
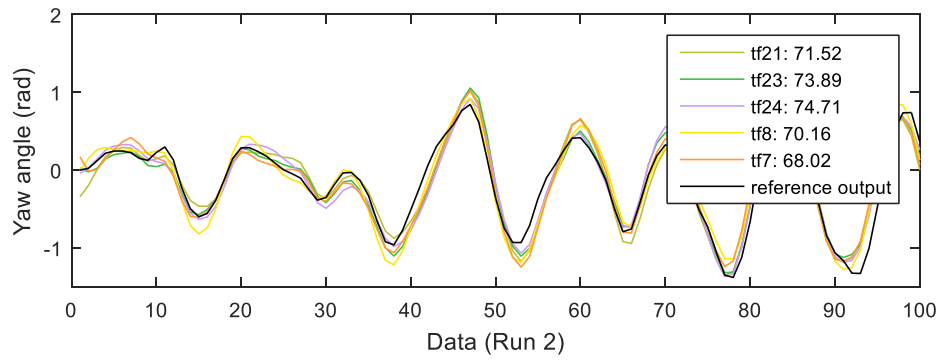
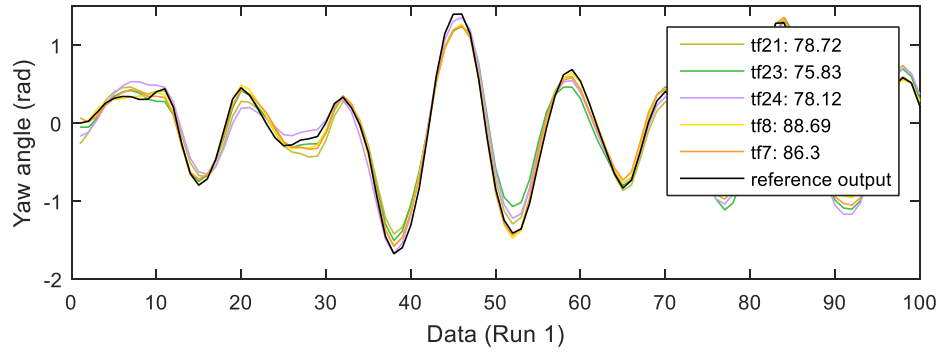


Figure 18: Measured and simulated model output for main yaw model

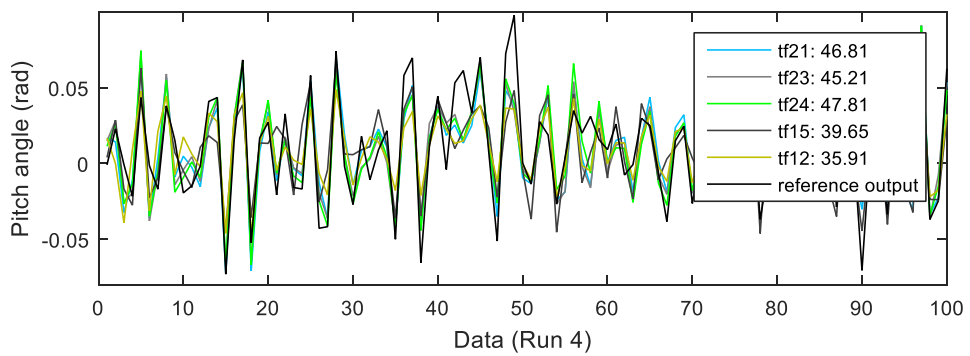
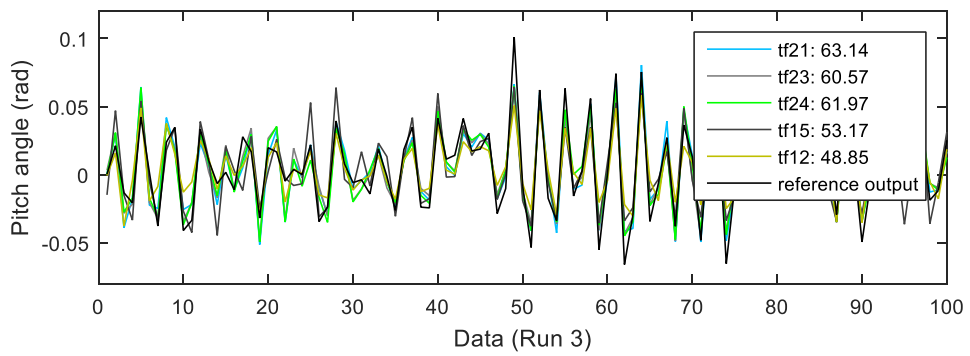
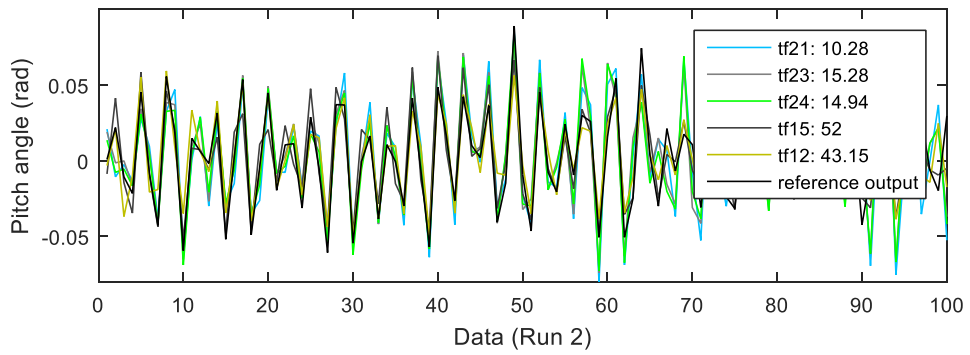
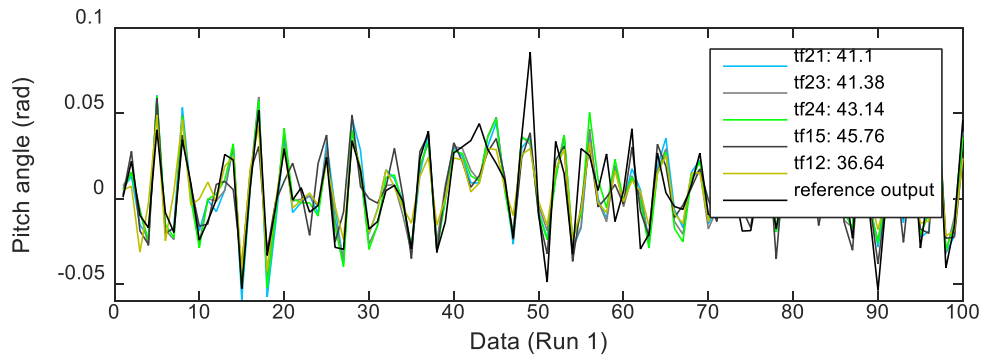


Figure 19: Measured and simulated model output for cross yaw model

4.1.5. Complete TRMS model

After inserting all the transfer functions found into respective sections, the complete TRMS model was formed as shown in **Figure 20**. The inputs to the system are input voltage to pitch rotor and input voltage to yaw rotor, while the outputs are pitch angle and yaw angle.

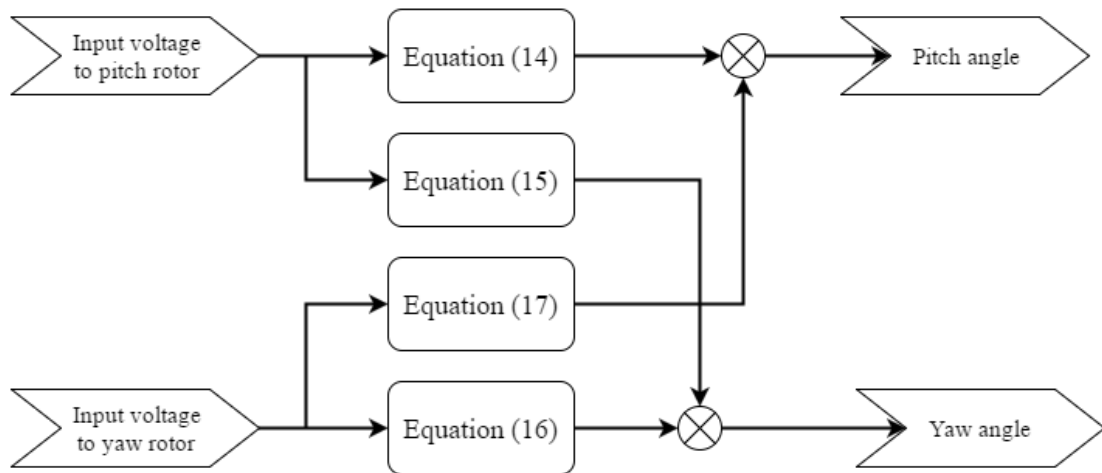


Figure 20: Complete TRMS model

4.2. Controller design

Once the complete model of TRMS was found, it was then used for design of PID controller and LQR controller. The controllers were first tested through simulation to observe the performance of the controllers on the system before implemented on real time system.

4.2.1. PID tuning

Ultimate gain that causes the system to oscillate upon a step response could not be achieved. Since Ziegler-Nichols closed-loop tuning was not applicable in TRMS, thus the PID gain parameters can only be determined through trial and error. All the

gain parameters (K_p , K_i , K_d) were started from 0 and increased slowly until a satisfying performance was achieved. In the end of trial and error, the parameters for pitch PID controller were found to be $K_p=3$, $K_i=3$, $K_d=6$ while the parameters for yaw PID controller were found to be $K_p=3$, $K_i=2$, $K_d=6$.

4.2.2. LQR tuning

As LQR only works with state-space model, state-space model of main pitch and main yaw were formed prior to design of LQR controller. By using the general equation for state-space model:

$$\frac{dx}{dt} = A x(t) + B u(t) \quad (18)$$

$$y(t) = C x(t) + D u(t) \quad (19)$$

The matrices of A,B,C and D for main pitch state-space model were found to be:

$$A = \begin{bmatrix} 0.0549 & -1.9496 & 0.1216 & 0.0761 & 0.4212 & 0.3368 & 0.1657 \\ 2.0063 & -0.131 & 0.0445 & -0.0744 & 0.1171 & 0.0563 & -0.05 \\ -0.12 & 0.1511 & -0.0855 & 5.1e-4 & -0.258 & -0.0999 & -0.2899 \\ 0.0165 & 0.4327 & -0.3402 & -0.0145 & 2.2527 & 0.4981 & -1.5312 \\ -0.2851 & -0.0032 & -0.2512 & -1.8968 & -0.9634 & -1.3883 & -1.1619 \\ 0.0395 & -0.2326 & 0.0984 & 0.2304 & 0.0062 & -1.0687 & -0.7015 \\ 0.0638 & -0.0808 & 0.0054 & 0.7786 & 0.5206 & 1.0897 & -1.0138 \end{bmatrix}$$

$$B = \begin{bmatrix} -0.5163 \\ -0.5322 \\ 0.2132 \\ 1.3387 \\ 1.3509 \\ -1.2631 \\ 0.5782 \end{bmatrix}$$

$$C = [0.8071 \quad -0.9136 \quad -9.336e-4 \quad -0.0755 \quad -0.0369 \quad -0.0148 \quad -0.0202]$$

$$D = [0]$$

The matrices of A,B,C and D for main yaw state-space model were found to be:

$$A = \begin{bmatrix} -0.0308 & 0.4427 & -0.0034 & -0.0089 & 0.0153 \\ -0.6069 & -0.0781 & -0.0694 & -0.0295 & -0.0919 \\ -0.077 & 0.1362 & -0.7998 & -1.0871 & -0.8408 \\ -0.0422 & -0.0424 & 0.9924 & 0.2261 & 1.3201 \\ -0.0202 & -0.0139 & 0.0523 & -1.4574 & 0.3355 \end{bmatrix}$$

$$B = \begin{bmatrix} -0.0163 \\ 0.1228 \\ -0.5058 \\ 0.1801 \\ 0.3846 \end{bmatrix}$$

$$C = [4.8761 \quad 0.7394 \quad -0.1535 \quad -0.0393 \quad 0.0066]$$

$$D = [0]$$

Matrix R was set as [1] while matrix Q was started with an identity matrix and further fine-tuned through trial and error. The final matrix Q and the resultant gain K for main pitch LQR controller were found to be:

$$Q = \begin{bmatrix} 100 & 0 & 0 & 0 & 0 & 0 & 0 \\ 0 & 20 & 0 & 0 & 0 & 0 & 0 \\ 0 & 0 & 0.01 & 0 & 0 & 0 & 0 \\ 0 & 0 & 0 & 1 & 0 & 0 & 0 \\ 0 & 0 & 0 & 0 & 1 & 0 & 0 \\ 0 & 0 & 0 & 0 & 0 & 0.01 & 0 \\ 0 & 0 & 0 & 0 & 0 & 0 & 0.01 \end{bmatrix}$$

$$K = [-1.6726 \quad -10.3326 \quad 0.2461 \quad -0.0179 \quad 0.5945 \quad 0.2637 \quad 0.2626]$$

while the final matrix Q and the resultant gain K for main pitch LQR controller were found to be:

$$Q = \begin{bmatrix} 10 & 0 & 0 & 0 & 0 \\ 0 & 1 & 0 & 0 & 0 \\ 0 & 0 & 1 & 0 & 0 \\ 0 & 0 & 0 & 1 & 0 \\ 0 & 0 & 0 & 0 & 1 \end{bmatrix}$$

$$K = [1.6814 \quad 1.4736 \quad -0.7545 \quad 0.0877 \quad 0.5908]$$

4.2.3. Simulation

The pitch PID controller corrects the error in term of differences between desired pitch angle and the exact pitch angle. At the yaw side, the yaw PID controller corrects the error in term of differences between desired yaw angle and the exact yaw angle. The 'TRMS model' block contains the complete TRMS model shown in **Figure 20**. Both setpoint and output for pitch angle and yaw angle were recorded in the scope for observation and analysis. In the simulation, the setpoint for pitch angle was set at 0.45 rad while the setpoint of yaw angle was set at 0.4 rad. The gain parameters found for PID were used for simulation and the calculated gain matrix, K, for LQR was

implemented into the LQR controller to work with PID controller in controlling the system. It can be seen that the output response of PID+LQR controller is better than that of PID-only controller. The performance of pitch rotor is considered as reliable, however, the yaw rotor is performing relatively poor. One possible reason for yaw rotor to take a longer time to reach steady state is due to the cross coupling effect from the pitch rotor.

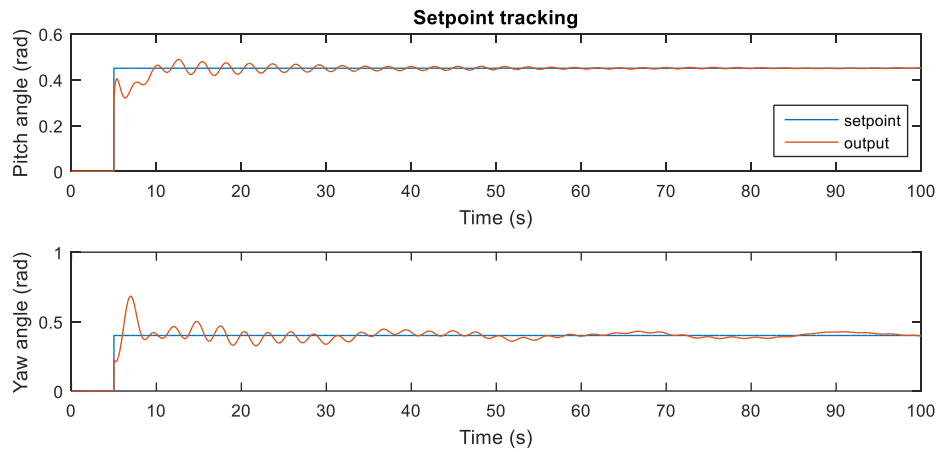


Figure 21: Setpoint tracking in simulation (PID)

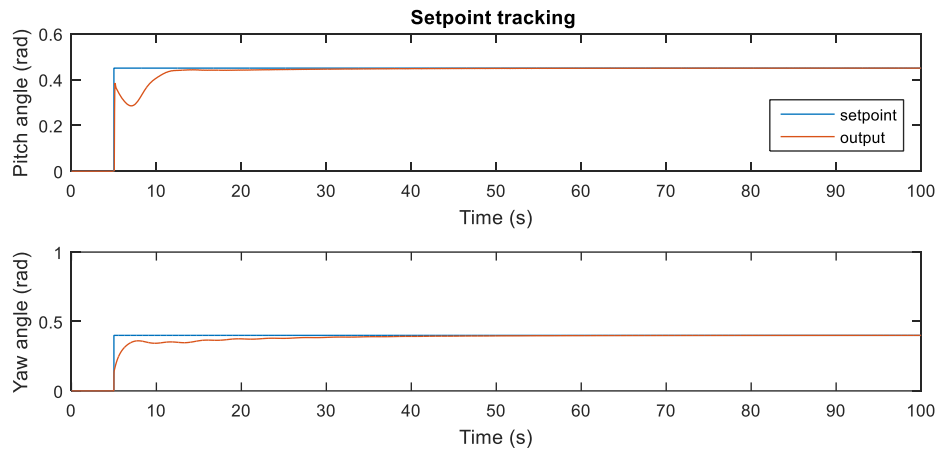


Figure 22: Setpoint tracking in simulation (PID+LQR)

4.3. Field test

A combination of PID controller and LQR controller were applied to TRMS in real-time and the results were recorded through the scope. The desired pitch angle was set at 0.45 rad while the desired yaw angle was set at 0.4 rad. In term of setpoint tracking, the overall performance in real-time is better than that in simulation. For pitch angle, the settling time is at around 8 seconds and the maximum overshoot is 30%. For yaw angle, the settling time is at around 9 seconds and the maximum overshoot is 92.5%. The high percentage overshoot is probably due to the cross-coupling effect from pitch rotor during step change from 0 to 0.45. For disturbance rejection, it was found that the overall performance of pitch rotor is satisfying while the yaw rotor is rejecting the disturbance slightly slower.

4.3.1. Setpoint tracking

Setpoint for pitch rotor was fixed at 0.45 rad while the setpoint for yaw rotor was fixed at 0.4 rad. Both of the setpoints were triggered by step inputs at 5th second. Based on the results obtained, it can be seen that the settling time for both cases are the same, just that PID-only controller is giving a smoother response. Thus, in term of setpoint tracking, PID-only controller is a better choice compared to PID+LQR controller.

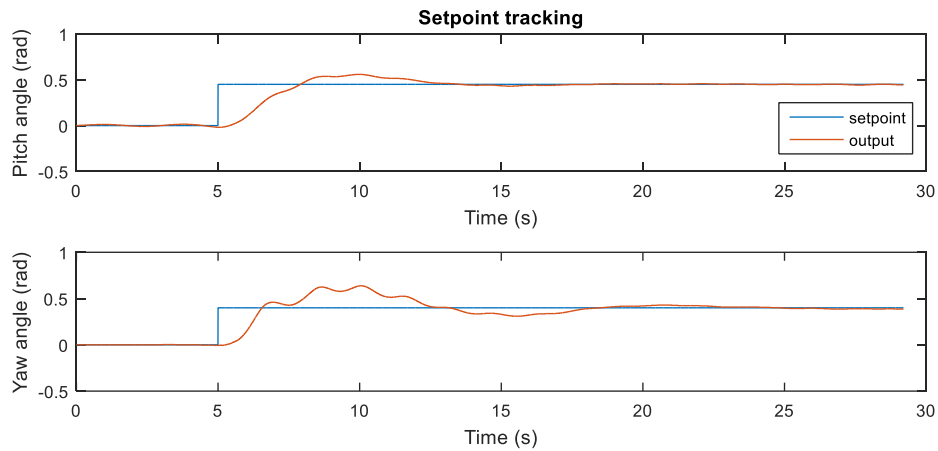


Figure 23: Setpoint tracking in real-time (PID)

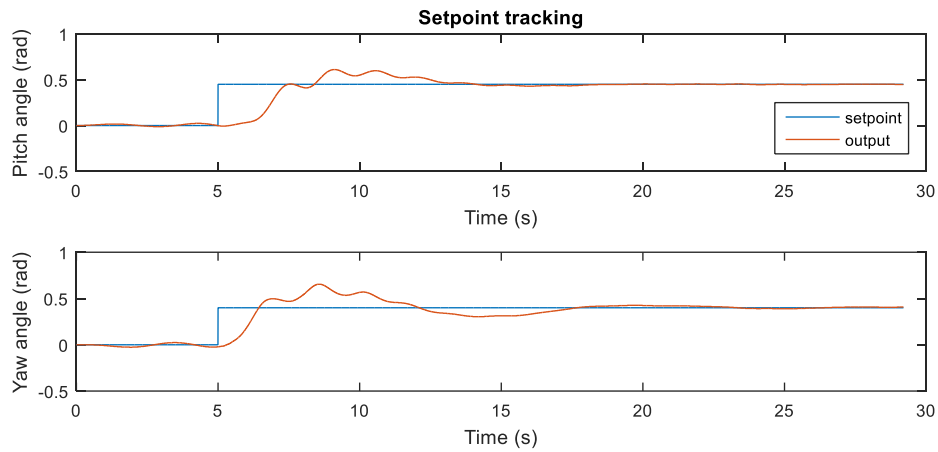


Figure 24: Setpoint tracking in real-time (PID+LQR)

4.3.2. Disturbance rejection part 1: wind source from x1 to x2

In this part of experiment, step inputs were applied to both pitch rotor and yaw rotor at 5th second. Wind from table fan was applied towards the side of pitch rotor at 30th second and it was elapsed for 20 seconds before the table fan was removed. Thus, the disturbance rejection response can be observed starting from 30th second. Based on the result, it was found that there is 25% improvement in term of overshoot during disturbance rejection in yaw PID+LQR controller compared to PID-only controller. By referring to the output response curve between 30th second and 60th second, we can say that PID+LQR controller gives a faster response in providing corrective action against the disturbance when compared to PID-only controller.

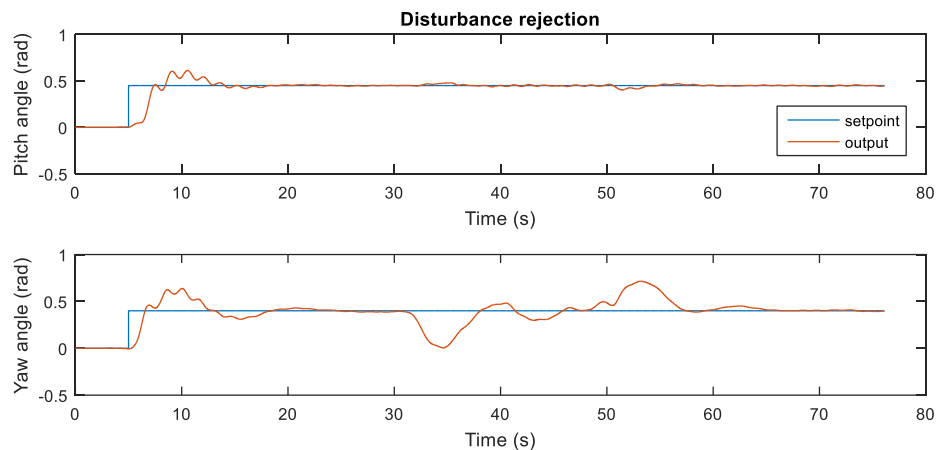


Figure 25: Disturbance rejection part 1 (PID)

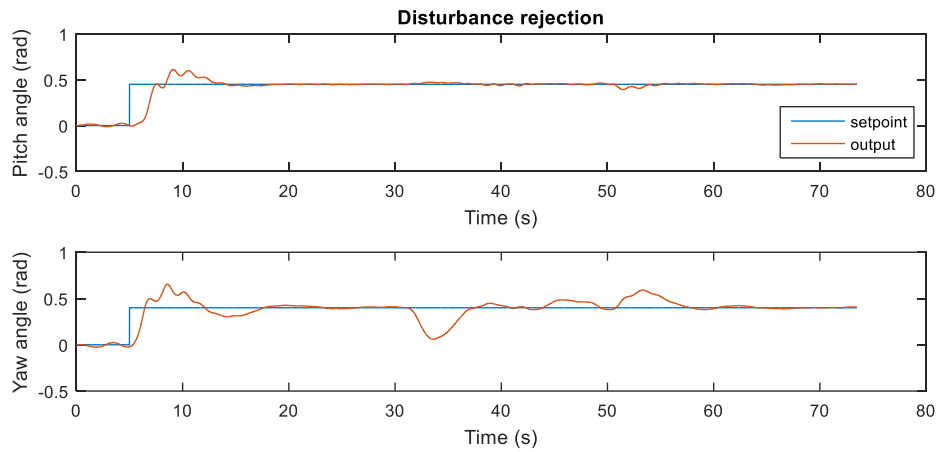


Figure 26: Disturbance rejection part 1 (PID+LQR)

4.3.3. Disturbance rejection part 2: wind source from z1 to z2

Step inputs were applied to both pitch rotor and yaw rotor at 5th second. Wind from table fan was applied towards the top of pitch rotor at 30th second and it was elapsed for 20 seconds before the table fan was removed. Through the observation on output response curve starting from 30th second, it was found that PID+LQR pitch controller is giving a 89% improvement in term of overshoot during disturbance rejection compared to PID-only controller. For yaw part, there is 33% improvement on PID+LQR controller compared to PID-only controller. Other than that, significant cross-coupling effect was observed at the yaw angle when the controller on pitch rotor was working to reject the disturbance.

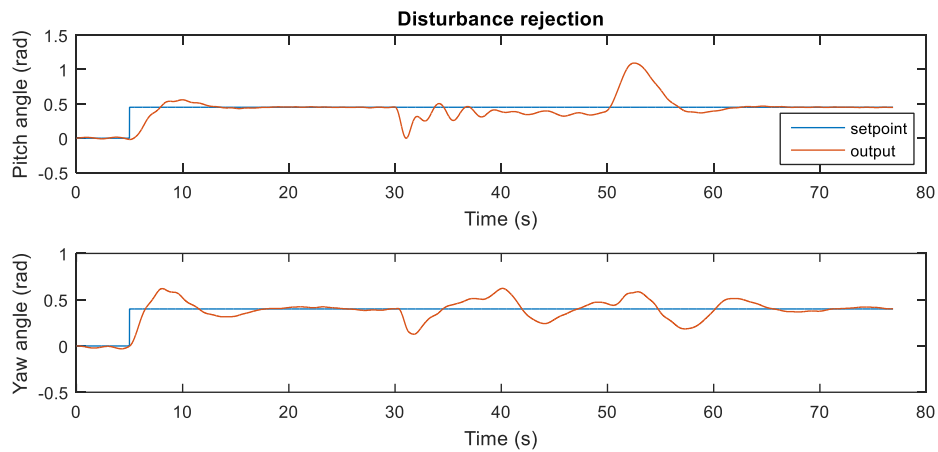


Figure 27: Disturbance rejection part 2 (PID)

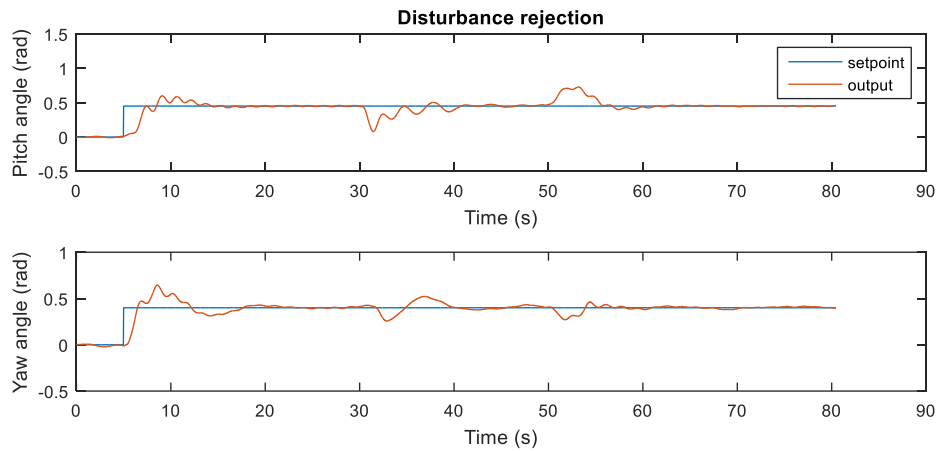


Figure 28: Disturbance rejection part 2 (PID+LQR)

4.3.4. Disturbance rejection part 3: wind source from x3 to x4

After step inputs were applied to both of the rotors at 5th second and the rotors were stabilized, wind from a table fan was applied towards the side of yaw rotor at 30th second and elapsed for 20 seconds before it was taken away from the TRMS. From the output response during disturbance rejection period, which is starting from 30th second, it can be seen that the output response from PID+LQR controller during disturbance rejection period is smoother than that of PID-only controller. This is probably because PID+LQR controller is using both states and output, thus giving a faster and continuous corrective action.

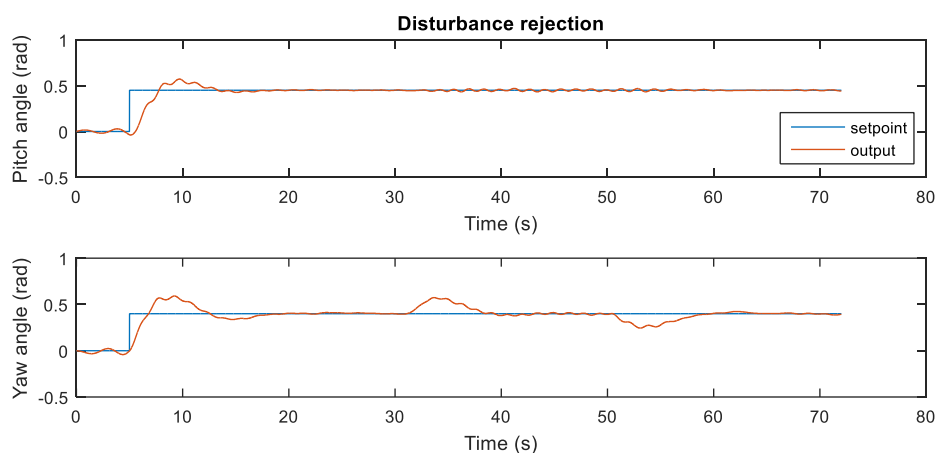


Figure 29: Disturbance rejection part 3 (PID)

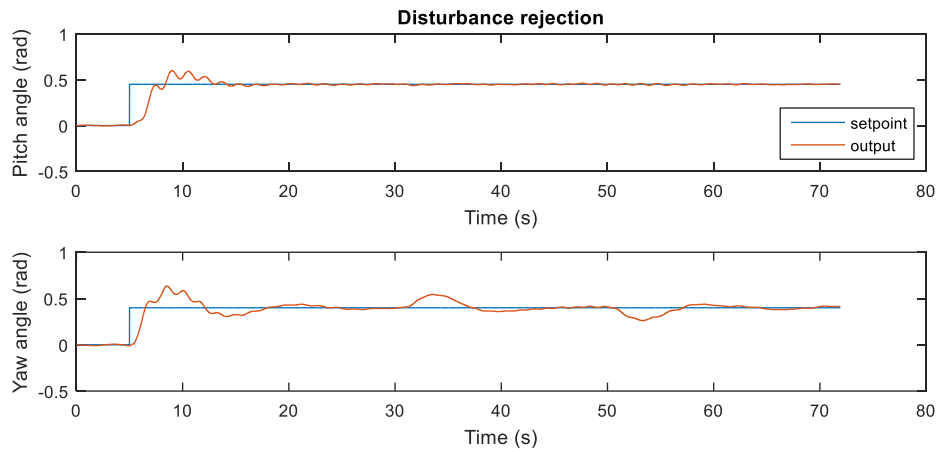


Figure 30: Disturbance rejection part 3 (PID+LQR)

4.3.5. Disturbance rejection part 4: wind source from z3 to z4

Step inputs were applied to both pitch rotor and yaw rotor at 5th second. Wind from table fan was applied towards the top of yaw rotor at 30th second and it was elapsed for 20 seconds before the table fan was removed. From the results obtained, it can be seen that there is not much effect on either pitch angle or yaw angle when the wind was introduced as a disturbance to the system. Thus, we can say that wind applied towards the top of yaw rotor is not creating much disturbance to the system.

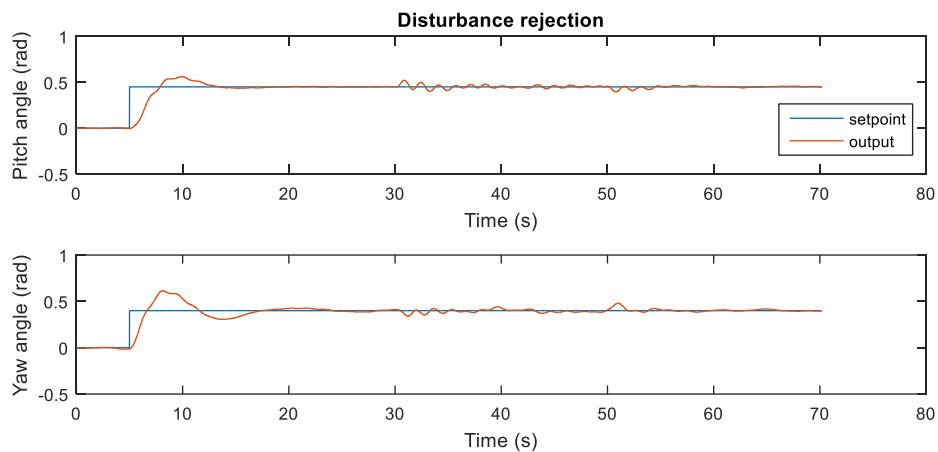


Figure 31: Disturbance rejection part 4 (PID)

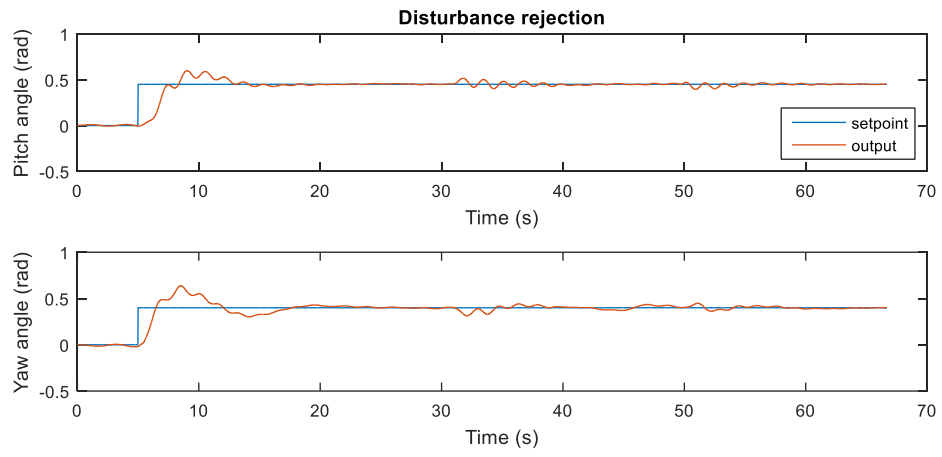


Figure 32: Disturbance rejection part 4 (PID+LQR)

CHAPTER 5

CONCLUSION

5. CONCLUSION

5.1. Conclusion

Complete TRMS model was formed through a series of experimentations. After the relationship curves between output voltage to the rotors and displacement angles were collected, the overall best transfer functions that can represent each subsystem were found and inserted to respective blocks to form the complete model. PID controller was designed based on the completed model while state-space models of pitch rotor and yaw rotor were further estimated for the design of LQR controller. Once the gain parameters of controllers were obtained, they were tested through simulation before implemented to the real-time system. From the results shown, it can be concluded that the controllers were giving reliable performance in term of setpoint tracking and disturbance rejection.

A sequence of methodology was proposed to design PID and LQR controllers to control TRMS against disturbance and set-point changes. It was found that the advantage of combining PID and LQR controllers is that the system is:

- stable – reach steady state in short period
- robust – able to reject disturbance in short period

Besides, PID and LQR are both easier to design compared to other techniques such as neural networks and fuzzy logic. With the resources available, the project was completed within given time frame. In the end of this project, the combination of PID and LQR controller was able to give optimal performance against disturbances and track given setpoint within short period.

5.2. Recommendations

As the overshoot in yaw rotor was found to be quite high, thus the yaw controllers can still be tuned to get better performance. Besides, the response from the model obtained seems to deviate from the actual system. This might be the drawback from the way of modelling through experimentation. The alternative to this is to model through derivations of mathematical expressions and physics laws. This project only covered disturbance rejection tests from x-axis and z-axis, it can still be extended to include y-axis or multiple axes at the same time. For better accuracy in the disturbance rejection test, wind tunnel can be used to provide a better simulation of wind effect on TRMS. Last but not least, the outcome of this project is not limited to implementation on TRMS, the methodology can be applied on other nonlinear MIMO systems with certain level of fine-tuning for optimization purpose.

REFERENCES

- [1] W. Johnson, *Helicopter Theory*: Dover Publications, 1980.
- [2] A. R. Bramwell, D. Balmford, and G. Done, *Bramwell's helicopter dynamics*: Butterworth-Heinemann, 2001.
- [3] J. Watkinson, "5 - The tail," in *Art of the Helicopter*, J. Watkinson, Ed., ed Oxford: Butterworth-Heinemann, 2004, pp. 166-190.
- [4] S. M. Ahmad, A. J. Chipperfield, and M. O. Tokhi, "Dynamic modeling and optimal control of a twin rotor MIMO system," in *National Aerospace and Electronics Conference, 2000. NAECON 2000. Proceedings of the IEEE 2000*, 2000, pp. 391-398.
- [5] D. Rotondo, F. Nejjari, and V. Puig, "Quasi-LPV modeling, identification and control of a twin rotor MIMO system," *Control Engineering Practice*, vol. 21, pp. 829-846, 6// 2013.
- [6] F. Aldebrez, I. M. Darus, and M. Tokhi, "Dynamic modelling of a twin rotor system in hovering position," in *Control, Communications and Signal Processing, 2004. First International Symposium on*, 2004, pp. 823-826.
- [7] P. Chalupa, J. Příklad, and J. Novák, "Modelling of Twin Rotor MIMO System," *Procedia Engineering*, vol. 100, pp. 249-258, 2015.
- [8] R. Christensen, N. Fogh, R. H. Hansen, M. S. Jensen, S. Larsen, and A. Paramanathan, "Modelling and Control of a Twin-Rotor MIMO System," Aalborg University, Denmark, 2006.
- [9] F. I. Ltd., "Twin Rotor MIMO System Control Experiments 33-949S," Feedback Instruments Ltd., Feedback Instruments Ltd., Park Road, Crowborough, East Sussex, TN6 2QX, UK, Manual, 2013.
- [10] M. Jahed and M. Farrokhi, "Robust adaptive fuzzy control of twin rotor MIMO system," *Soft Computing*, vol. 17, pp. 1847-1860, 2013.
- [11] A. Rahideh, A. H. Bajodah, and M. H. Shaheed, "Real time adaptive nonlinear model inversion control of a twin rotor MIMO system using neural networks," *Engineering Applications of Artificial Intelligence*, vol. 25, pp. 1289-1297, 9// 2012.
- [12] A. Ramalakshmi and P. Manoharan, "Non-linear modeling and PID control of twin rotor MIMO system," in *Advanced Communication Control and Computing Technologies (ICACCCT), 2012 IEEE International Conference on*, 2012, pp. 366-369.
- [13] C. W. Tao, J. S. Taur, Y. H. Chang, and C. W. Chang, "A Novel Fuzzy-Sliding and Fuzzy-Integral-Sliding Controller for the Twin-Rotor Multi-Input–Multi-Output System," *IEEE Transactions on Fuzzy Systems*, vol. 18, pp. 893-905, 2010.
- [14] S. Mondal and C. Mahanta, "Adaptive second-order sliding mode controller for a twin rotor multi-input-multi-output system," *IET Control Theory & Applications*, vol. 6, pp. 2157-2167, 2012.
- [15] S. Juhng-Perng, L. Chi-Ying, and C. Hung-Ming, "Robust control of a class of nonlinear systems and its application to a twin rotor MIMO system," in *Industrial Technology, 2002. IEEE ICIT '02. 2002 IEEE International Conference on*, 2002, pp. 1272-1277 vol.2.
- [16] F. Allgower, R. Findeisen, and Z. K. Nagy, "Nonlinear model predictive control: from theory to application," *Journal of the Chinese Institute of Chemical Engineers*, vol. 35, pp. 299-315, 2004.
- [17] T. A. Johansen, "Introduction to nonlinear model predictive control and moving horizon estimation," *Selected Topics on Constrained and Nonlinear Control*, pp. 1-53, 2011.
- [18] T. A. Badgwell and S. J. Qin, "Review of nonlinear model predictive control applications," *Non-Linear Predictive Control: Theory and Practice*, p. 1, 2001.

- [19] Š. PAVEL, "NONLINEAR MIMO SYSTEM CONTROL USING NONLINEAR PREDICTIVE CONTROLLER," in *9th International Conference PROCESS CONTROL 2010*, Kouty nad Desnou, Czech Republic, 2010.
- [20] L. Imsland, R. Findeisen, E. Bullinger, F. Allgöwer, and B. A. Foss, "A note on stability, robustness and performance of output feedback nonlinear model predictive control," *Journal of Process Control*, vol. 13, pp. 633-644, 2003.
- [21] A. Grancharova and T. A. Johansen, "Nonlinear model predictive control," in *Explicit Nonlinear Model Predictive Control*, ed: Springer, 2012, pp. 39-69.
- [22] M. A. Henson, "Nonlinear model predictive control: current status and future directions," *Computers & Chemical Engineering*, vol. 23, pp. 187-202, 1998.
- [23] R. Findeisen, L. Imsland, F. Allgower, and B. A. Foss, "State and output feedback nonlinear model predictive control: An overview," *European journal of control*, vol. 9, pp. 190-206, 2003.
- [24] A. K. Agrawal, "Optimal Controller Design for Twin Rotor MIMO System," 2013.
- [25] C. Jaen, J. Pou, R. Pindado, V. Sala, and J. Zaragoza, "A Linear-Quadratic Regulator with Integral Action Applied to PWM DC-DC Converters," in *IECON 2006 - 32nd Annual Conference on IEEE Industrial Electronics*, 2006, pp. 2280-2285.
- [26] J. Luo and C. E. Lan, "Determination of weighting matrices of a linear quadratic regulator," *Journal of Guidance, Control, and Dynamics*, vol. 18, pp. 1462-1463, 1995.
- [27] A. Q. Khan and N. Iqbal, "Modeling and Design of an Optimal Regulator for Three Degree of Freedom Helicopter/Twin Rotor Control System," in *Engineering, Sciences and Technology, Student Conference On*, 2004, pp. 45-50.

APPENDICES

A.1. Project timeline and key milestones

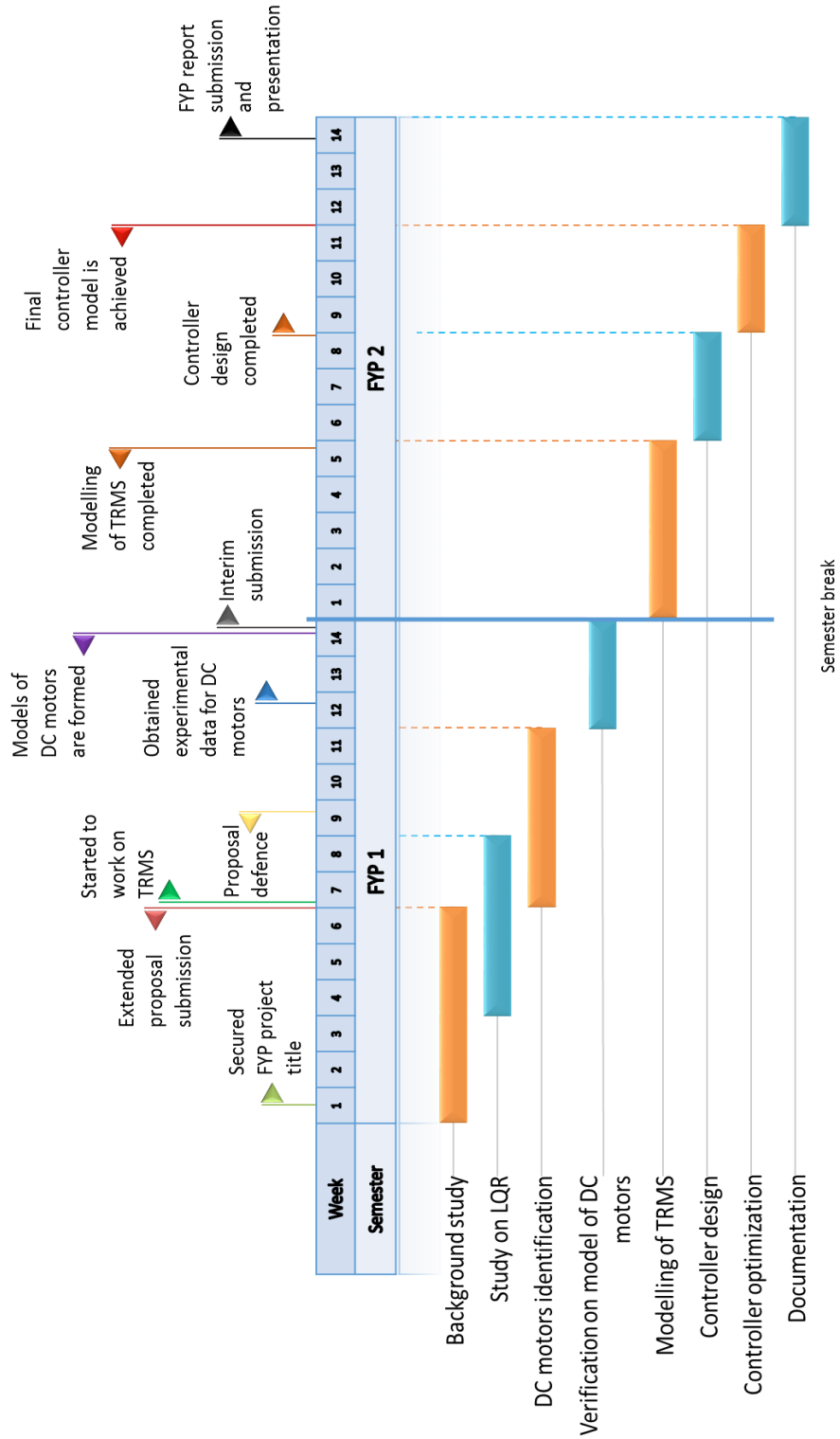


Figure A - 1: Project Timeline and Key Milestones

A.2. Data collected from main rotor

Table A - 1 shows the data obtained after applying increasing step input from 0V to 5V with 0.2V step to the main rotor. From **Figure A - 2**, it can be seen that there is not much variation between the output given from digital tachometer and DC tachometer. By taking the sign in count, the magnitudes of angular velocity of main rotor is proportional to the input voltages.

Table A - 1: Data collected from main rotor experiment

Output signal from PC (Volt)	Signed signal from PC (Volt)	Input voltage to rotor (Volt)	Digital tachometer		DC tachometer		
			Rotational speed (RPM)	Angular velocity (rad/s)	Output voltage (Volt)	Rotational speed (RPM)	Angular velocity (rad/s)
0	-2.5	20.21	-2528	-264.73	-1.5	-2884.62	-302.08
0.2	-2.3	19.17	-2464	-258.03	-1.45	-2788.46	-292.01
0.4	-2.1	17.71	-2370	-248.19	-1.39	-2673.08	-279.92
0.6	-1.9	16.18	-2244	-234.99	-1.33	-2557.69	-267.84
0.8	-1.7	14.66	-2107	-220.64	-1.25	-2403.85	-251.73
1	-1.5	13.13	-1987	-208.08	-1.18	-2269.23	-237.63
1.2	-1.3	11.6	-1849	-193.63	-1.1	-2115.38	-221.52
1.4	-1.1	10.08	-1702	-178.23	-1.01	-1942.31	-203.40
1.6	-0.9	8.55	-1536	-160.85	-0.92	-1769.23	-185.27
1.8	-0.7	7	-1410	-147.65	-0.83	-1596.15	-167.15
2	-0.5	5.43	-1173	-122.84	-0.7	-1346.15	-140.97
2.2	-0.3	3.8	-909	-95.19	-0.54	-1038.46	-108.75
2.4	-0.1	1.79	-496	-51.94	-0.3	-576.92	-60.42
2.6	0.1	-1.17	330	34.56	0.196	376.92	39.47
2.8	0.3	-3.36	812	85.03	0.48	923.08	96.66
3	0.5	-5.02	1104	115.61	0.655	1259.62	131.91
3.2	0.7	-6.58	1333	139.59	0.786	1511.54	158.29
3.4	0.9	-8.12	1537	160.95	0.91	1750.00	183.26
3.6	1.1	-9.67	1702	178.23	1.008	1938.46	203.00
3.8	1.3	-11.19	1856	194.36	1.097	2109.62	220.92
4	1.5	-12.68	2009	210.38	1.18	2269.23	237.63
4.2	1.7	-14.19	2164	226.61	1.267	2436.54	255.15
4.4	1.9	-15.73	2287	239.49	1.345	2586.54	270.86
4.6	2.1	-17.31	2387	249.97	1.397	2686.54	281.33
4.8	2.3	-18.89	2458	257.40	1.456	2800.00	293.22
5	2.5	-20.07	2543	266.30	1.49	2865.38	300.06

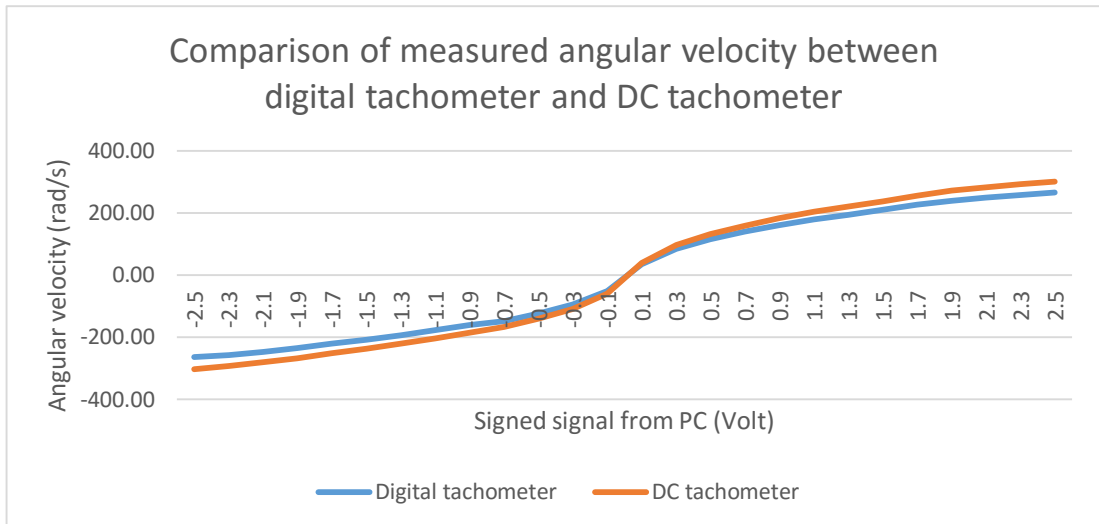


Figure A - 2: Comparison of measured angular velocity between digital tachometer and DC tachometer

A.3. Data collected from tail rotor

Table A - 2 shows the data obtained after applying increasing step input from 0V to 5V with 0.2V step to the tail rotor. From **Figure A - 3**, it can be seen that there is not much variation between the output given from digital tachometer and DC tachometer. By taking the sign in count, the magnitudes of angular velocity of tail rotor is proportional to the input voltages.

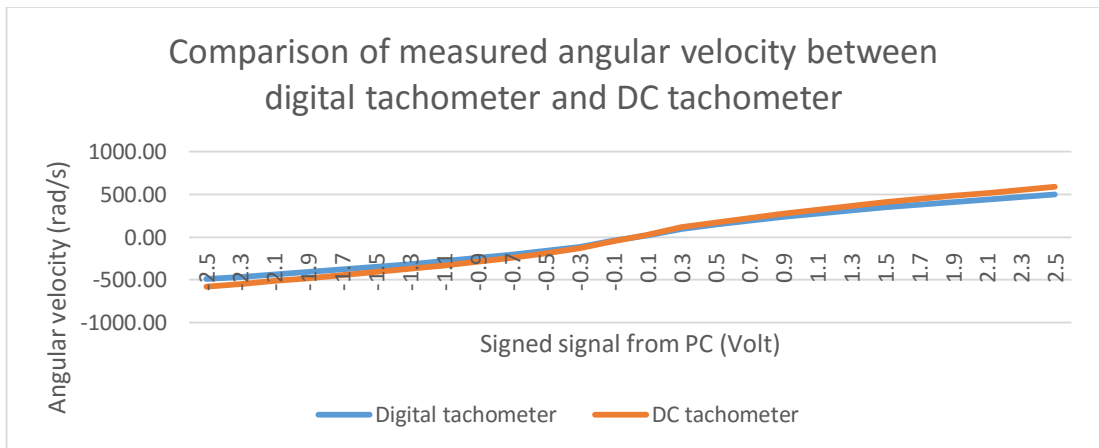


Figure A - 3: Comparison of measured angular velocity between digital tachometer and DC tachometer

Table A - 2: Data collected from main rotor experiment

Output signal from PC (Volt)	Signed signal from PC (Volt)	Input voltage to rotor (Volt)	Digital tachometer		DC tachometer		
			Rotational speed (RPM)	Angular velocity (rad/s)	Output voltage (Volt)	Rotational speed (RPM)	Angular velocity (rad/s)
0	-2.5	-15.37	-4699	-492.08	-2.89	-5557.69	-582.00
0.2	-2.3	-14.26	-4488	-469.98	-2.736	-5261.54	-550.99
0.4	-2.1	-13.17	-4184	-438.15	-2.565	-4932.69	-516.55
0.6	-1.9	-12.09	-3938	-412.39	-2.394	-4603.85	-482.11
0.8	-1.7	-11.01	-3645	-381.70	-2.21	-4250.00	-445.06
1	-1.5	-9.91	-3361	-351.96	-2.042	-3926.92	-411.23
1.2	-1.3	-8.81	-3064	-320.86	-1.862	-3580.77	-374.98
1.4	-1.1	-7.71	-2701	-282.85	-1.647	-3167.31	-331.68
1.6	-0.9	-6.582	-2327	-243.68	-1.427	-2744.23	-287.38
1.8	-0.7	-5.438	-1955	-204.73	-1.192	-2292.31	-240.05
2	-0.5	-4.254	-1527	-159.91	-0.945	-1817.31	-190.31
2.2	-0.3	-2.983	-1077	-112.78	-0.655	-1259.62	-131.91
2.4	-0.1	-1.304	-423	-44.30	-0.255	-490.38	-51.35
2.6	0.1	0.775	214	22.41	0.132	253.85	26.58
2.8	0.3	2.604	886	92.78	0.559	1075.00	112.57
3	0.5	3.937	1392	145.77	0.85	1634.62	171.18
3.2	0.7	5.132	1830	191.64	1.115	2144.23	224.54
3.4	0.9	6.284	2227	233.21	1.366	2626.92	275.09
3.6	1.1	7.41	2622	274.58	1.585	3048.08	319.19
3.8	1.3	8.53	2963.5	310.34	1.813	3486.54	365.11
4	1.5	9.63	3317.5	347.41	2.02	3884.62	406.80
4.2	1.7	10.72	3635	380.66	2.215	4259.62	446.07
4.4	1.9	11.82	3937.5	412.33	2.385	4586.54	480.30
4.6	2.1	12.88	4222.5	442.18	2.566	4934.62	516.75
4.8	2.3	13.96	4511	472.39	2.742	5273.08	552.20
5	2.5	15.02	4765.5	499.04	2.916	5607.69	587.24

A.4. Model identification of rotors

Based on the data collected, transfer function model and state-space model were formed to represent the rotors. The reasons for choosing both transfer function and state-space are as follows:

- they are the most commonly used models
- they are compatible to each other
- they are user-friendly for implementation in Simulink

A.4.1. Transfer function model of main rotor

Mathematical model of a DC motor is a first order transfer function and it is in the form of:

$$\frac{\Omega(s)}{U(s)} = \frac{K_t}{JRs + R(2D\bar{\omega}_a + B) + K_b K_t} \quad (20)$$

In reference to the mathematical model, 5 variants of first order transfer function models were estimated based on the data obtained from experiment. First order transfer function models were formed by setting the number of zeros always less than number of poles by 1. From the best fits scores shown in **Figure A - 4**, it can be seen that tf4 with 4 poles and 3 zeros is the best representation of main rotor.

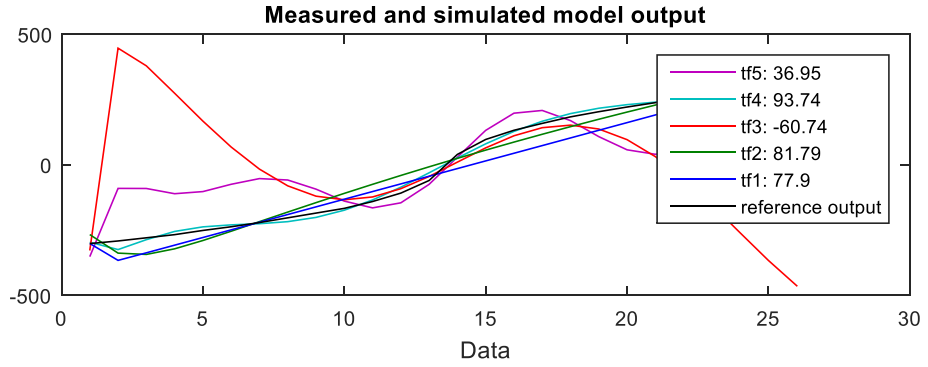


Figure A - 4: Transfer function models of main rotor

$$tf1 = \frac{790.4}{s+5.389} \quad (21)$$

$$tf2 = \frac{138.9s-3.581}{s^2+0.8943s+2.409e-11} \quad (22)$$

$$tf3 = \frac{-374.4s^2-8.266s-43.85}{s^3+3.363s^2+0.1009s+0.3393} \quad (23)$$

$$tf4 = \frac{257.6s^3+12.98s^2+52.71s-2.011}{s^4+1.945s^3+0.4033s^2+0.3402s+7.088e-8} \quad (24)$$

$$tf5 = \frac{-30.63s^4+22.85s^3-13.65s^2+10.27s+3.684}{s^5+1.622s^4+0.7089s^3+1.089s^2+0.08701s+0.1077} \quad (25)$$

A.4.2. State-space model for main rotor

4 variants of state-space models in the form of Equation (18) and Equation (19) were estimated based on the data obtained from experiment. The state-space model was formed with 1st order (ss1) and continued for higher orders (ss2, ss3 and ss4). It was found that 3rd order and 4th order state-space models (ss3 and ss4) are giving deteriorated responses, while second order state-space model (ss2) is the best representation of main rotor.

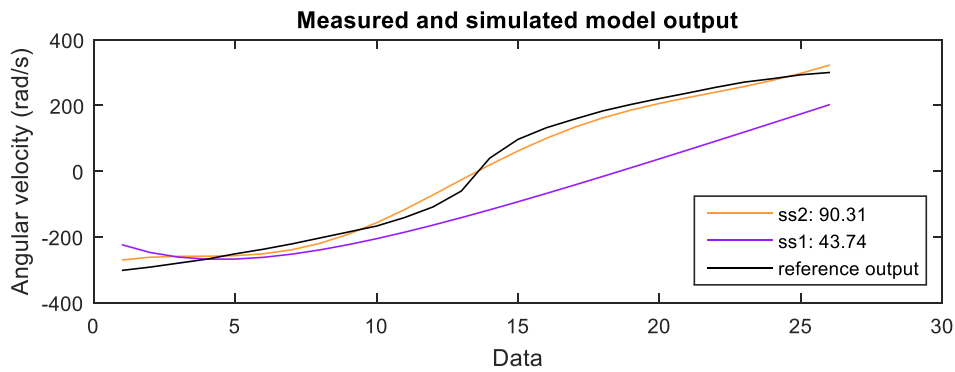


Figure A - 5: State-space models of main rotor (ss1 & ss2)

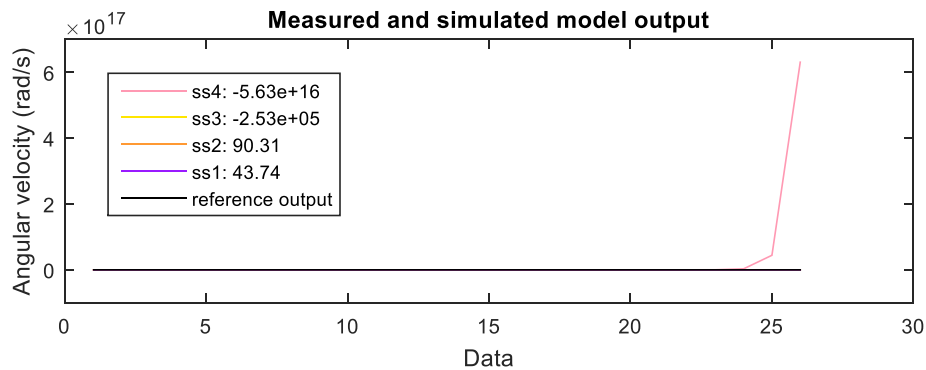


Figure A - 6: State-space models of main rotor (ss1, ss2, ss3 & ss4)

The values for matrices A, B, C and D were shown below-

ss1:

$$A = [-0.2061]$$

$$B = [0.153]$$

$$C = [189.2]$$

$$D = [0]$$

ss2:

$$A = \begin{bmatrix} -0.1305 & -0.4846 \\ 0.264 & 0.03235 \end{bmatrix}$$

$$B = \begin{bmatrix} -0.06725 \\ 0.2024 \end{bmatrix}$$

$$C = [-177.6 \quad 40.85]$$

$$D = [0]$$

ss3:

$$A = \begin{bmatrix} -0.157 & 0.1843 & 0.5556 \\ -0.5019 & 0.2298 & -0.2001 \\ 0.1074 & -0.131 & 0.387 \end{bmatrix}$$

$$B = \begin{bmatrix} 3.416e + 10 \\ -9.843e + 10 \\ 7.943e + 10 \end{bmatrix}$$

$$C = [133.9 \quad 66.24 \quad 3.349]$$

$$D = [0]$$

ss4:

$$A = \begin{bmatrix} -0.07826 & -0.2118 & -0.04416 & -0.8143 \\ 0.3492 & -0.006005 & -0.6944 & 0.5755 \\ 0.3133 & 0.8049 & 2.178 & 0.957 \\ 0.5237 & 0.5048 & 2.331 & -0.4661 \end{bmatrix}$$

$$B = \begin{bmatrix} -1679 \\ 2268 \\ 71.81 \\ -2697 \end{bmatrix}$$

$$C = [90.21 \quad -103.2 \quad 21.18 \quad -24.13]$$

$$D = [0]$$

A.4.3. Transfer function model for tail rotor

By matching the first order mathematical model shown in Equation (20), 5 variants of first order transfer function models were estimated based on the data obtained from experiment. First order transfer function models were formed by setting the number of zeros always less than number of poles by 1. From the best fits scores shown in **Figure A - 7**, it can be seen that tf4 with 4 poles and 3 zeros is the best representation of tail rotor.

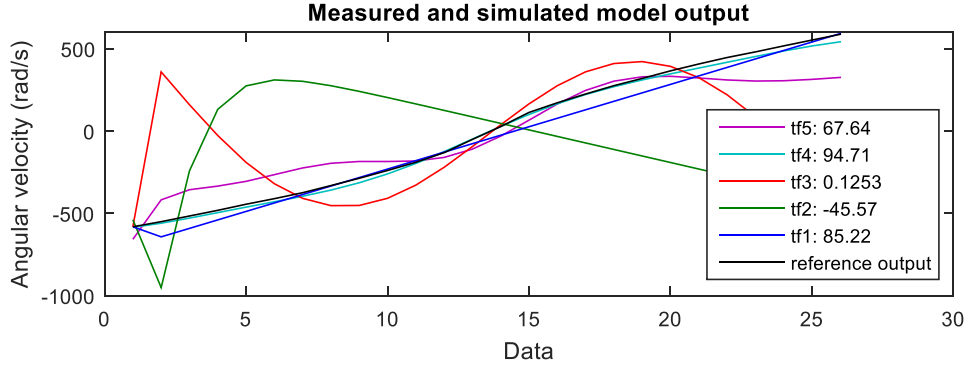


Figure A - 7: Transfer function models of tail rotor

$$tf1 = \frac{1957}{s+7.608} \quad (26)$$

$$tf2 = \frac{-189.3s-377}{s^2+3.024s+1.903} \quad (27)$$

$$tf3 = \frac{-1343s^2-56.28s-95.18}{s^3+10.19s^2+0.2697s+0.7629} \quad (28)$$

$$tf4 = \frac{-11.94s^3+61.56s^2+3.301s+2.21}{s^4+0.08493s^3+0.3583s^2+0.01358s+0.01225} \quad (29)$$

$$tf5 = \frac{-305.2s^4+136.6s^3+41.97s^2+15.96s+8.364}{s^5+1.155s^4+0.6834s^3+0.6076s^2+0.06527s+0.05452} \quad (30)$$

A.4.4. State-space model for tail rotor

3 variants of state-space models were estimated based on the data obtained from experiment. The state-space model was formed with 1st order (ss5) and continued for higher orders (ss6 and ss7). It was found that 1st order state-space model is giving a deteriorated response and second order state-space model (ss6) is the best representation of main rotor.

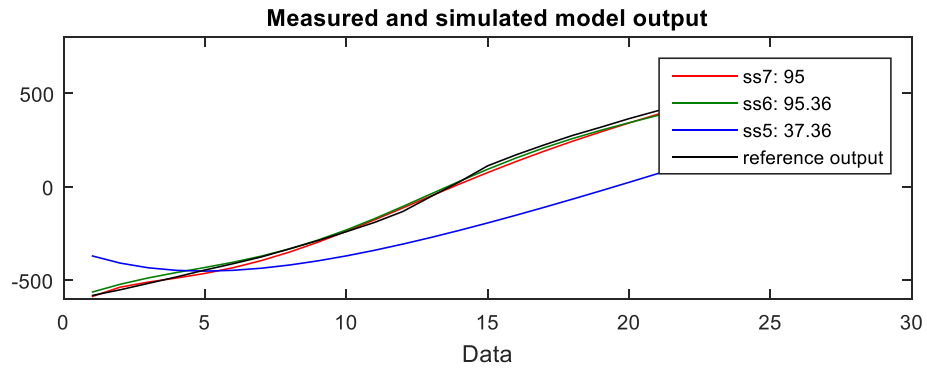


Figure A - 8: State-space models of tail rotor

By using the Equation (18) and Equation (19), the values for matrices A, B, C and D were shown below-

ss5:

$$A = [-0.1672]$$

$$B = [0.256]$$

$$C = [162.5]$$

$$D = [0]$$

ss6:

$$A = \begin{bmatrix} -0.07132 & -0.4595 \\ 0.3135 & 0.004896 \end{bmatrix}$$

$$B = \begin{bmatrix} -0.1017 \\ 0.5207 \end{bmatrix}$$

$$C = [-151 \quad 35.63]$$

$$D = [0]$$

ss7:

$$A = \begin{bmatrix} -0.06635 & -0.4722 & -0.6746 \\ 0.2601 & 0.144 & -0.05827 \\ 0.3492 & -0.01879 & -1.14 \end{bmatrix}$$

$$B = \begin{bmatrix} -0.4493 \\ -0.4336 \\ -1.01 \end{bmatrix}$$

$$C = [89.29 \quad -56.34 \quad -9.481]$$

$$D = [0]$$